ISPRS Journal of Photogrammetry and Remote Sensing 203 (2023) 71–85

Contents lists available at ScienceDirect

ISPRS Journal of Photogrammetry and Remote Sensing

journal homepage: www.elsevier.com/locate/isprsjprs

# Empirical insights on the use of sun-induced chlorophyll fluorescence to estimate short-term changes in crop transpiration under controlled water limitation

Kazi Rifat Ahmed [a,*], Eugenie Paul-Limoges [a], Uwe Rascher [b], Jan Hanus [c], Franco Miglietta [d], Roberto Colombo [e], Alessandro Peressotti [f], Andrea Genangeli [d], Alexander Damm [a,g]

[a] Department of Geography, University of Zurich, Winterthurerstrasse 190, 8057 Zurich, Switzerland
[b] Institute of Bio- and Geosciences, Plant Sciences (IBG-2), Forschungszentrum Jülich GmbH, 52428 Jülich, Germany
[c] Global Change Research Institute – CzechGlobe, Czech Academy of Sciences, Bělidla 986/4a, 60300 Brno, Czech Republic
[d] Institute of Bioeconomy – IBE, National Research Council – CNR, Via Caproni 8, 50145 Florence, Italy
[e] Department of Earth and Environmental Sciences, University of Milano Bicocca, Milano, Italy
[f] Department of Agricultural, Food, Environmental and Animal Sciences, University of Udine, Via delle Scienze 206, 33100 Udine, Italy
[g] Swiss Federal Institute of Aquatic Science and Technology, Surface Waters – Research and Management, Überlandstrasse 133, 8600 Dübendorf, Switzerland

ARTICLE INFO

*Keywords:*
Transpiration
Sun-induced chlorophyll fluorescence
Penman-Monteith
Ball-Berry-Leuning
Airborne optical data
Airborne thermal data

ABSTRACT

Knowledge of actual crop transpiration (T) is important for advanced crop management but challenging to obtain due to the large spatial and temporal variation of T. Remote sensing offers various possibilities to assess T dynamics, while particularly sun-induced chlorophyll fluorescence (SIF) has been demonstrated as a sensitive empirical proxy for T. Despite this success, the advancement of the mechanistic understanding of how SIF relates to T dynamics is key for the future development and implementation of robust and reliable SIF-based T products. This study aims to contribute insights by experimentally assessing the sensitivity of several SIF-based T estimation strategies for evolving soil water limitation. We investigated extensive in situ and airborne data acquired during a water limitation experiment in a maize canopy in northern Italy. We evaluated five empirical strategies to integrate SIF in a T modelling framework based on the Penman-Monteith (PM) and the Ball-Berry-Leuning (BBL) concepts. Our results indicate that replacing model parameters sensitive to canopy conductance with SIF results in the best agreement between modelled and measured T under evolving water limitation. Our study contributes expanding existing knowledge with empirical insights on the sensitivity of SIF based T approaches under increasing soil water limitation at short time scales.

## 1. Introduction

The occurrence of extreme climate events (e.g. droughts, heatwaves) substantially affects the ecosystem exchange of energy and water (Reichstein et al., 2002) and of carbon dioxide ($CO_2$) (Gharun et al., 2020; Reichstein et al., 2013; Sippel et al., 2018; Ramonet et al., 2020), and causes various feedbacks between the atmosphere and the biosphere (Anderegg et al., 2012; Bonan, 2008). Particularly the large deviation of abiotic drivers from their normal state under extreme conditions affects important plant exchange processes including gross primary productivity (GPP) (Frank et al., 2015; Gharun et al., 2020) and transpiration (T) (He et al., 2022), thus, substantially impacts the energy, water and carbon balance of entire ecosystems. Robust and accurate T and GPP estimates at appropriate spatio-temporal scales, together with underlying abiotic and biotic drivers, are essential to understand the complex energy-water-carbon relation of plants (Gentine et al., 2019) and help gaining insights on plant responses to extreme weather and changing environmental conditions.

Remote sensing (RS) is well suited to provide spatially harmonized and across scale information on ecosystem state and functioning (Xiao et al., 2021). However, due to the nature of RS data available for information retrieval (i.e. top-view perspective (Damm et al., 2020), measurement of light absorption, scattering and emission, discontinuous temporal sampling of polar-orbiting satellites (Xiao et al., 2021)), estimates of the subtle and complex carbon and water exchange processes remains highly challenging. This is even more so since ecosystem

* Corresponding author.
*E-mail address:* rifat.ahmed@geo.uzh.ch (K.R. Ahmed).

https://doi.org/10.1016/j.isprsjprs.2023.07.016
Received 20 January 2023; Received in revised form 8 July 2023; Accepted 14 July 2023
Available online 31 July 2023

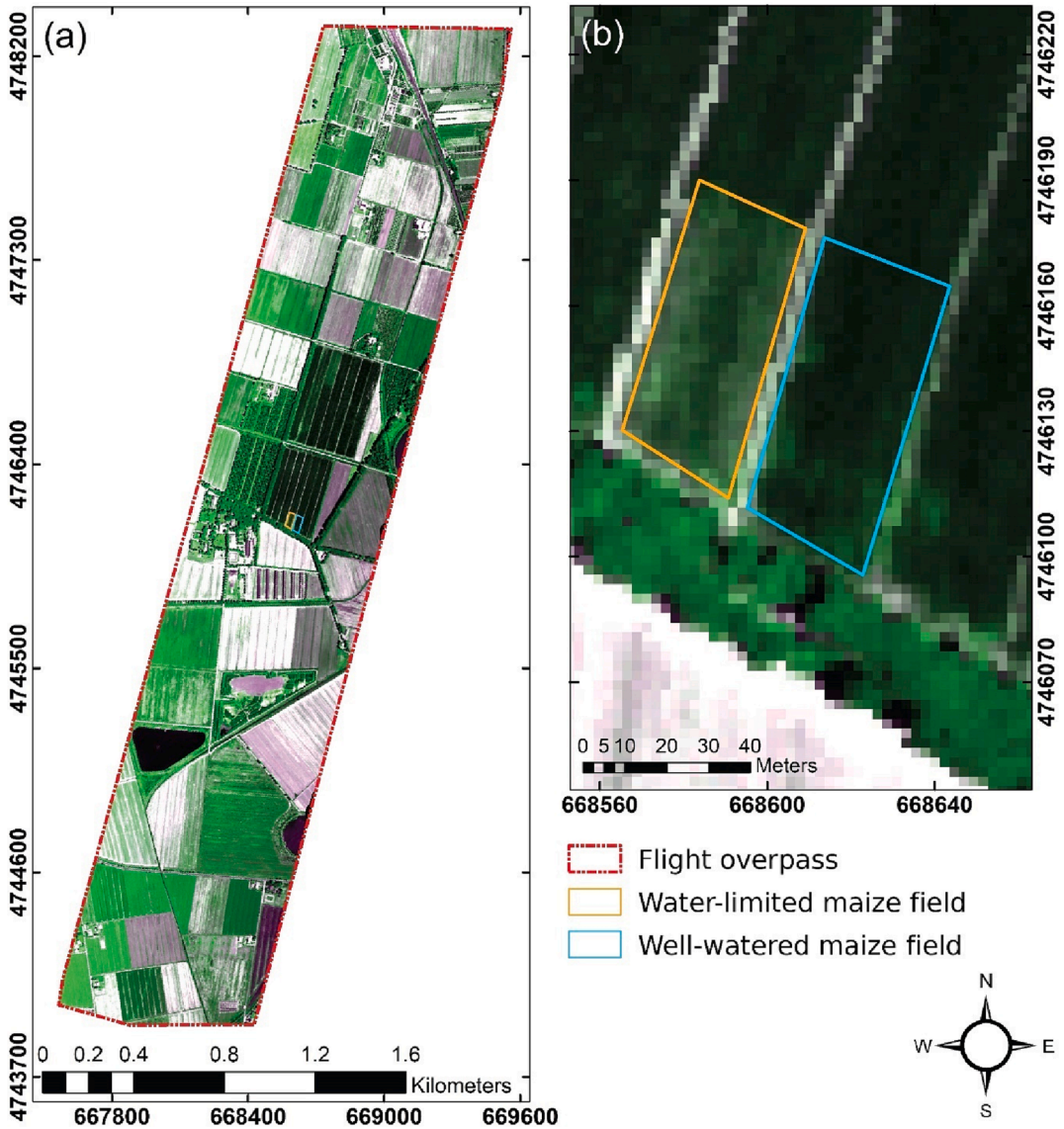


**Fig. 1.** False-color composite of the study area measured with the HyPlant imaging spectrometer - (a) test site with its surrounding and (b) the core experimental site comprising two maize areas. Data was acquired on 24 June 2019.

processes are determined by a complex set of abiotic and biotic drivers (GPP e.g. by light energy, ambient $CO_2$ availability or plant type; T e.g. by energy, atmospheric water vapour, and physiological constraints). Concerning GPP, substantial advancement has been made in RS based GPP estimates over the past decade (cf. Ryu et al., 2019), particularly stimulated by the increasing availability of RS derived sun-induced chlorophyll fluorescence (SIF) information (Gentine et al., 2019; Mohammed et al., 2019; Porcar-Castell et al., 2021; Schimel et al., 2019). A demonstration of improved global GPP estimates via time series of spatially downscaled SIF is presented in (Wang et al., 2022).

The subtle T process cannot be directly measured via RS, consequently, most proposed T methods rely on RS proxies of abiotic and biotic factors that are combined with models (e.g. Hilker et al., 2013; Langensiepen et al., 2009; Yebra et al., 2013). This indicates that the robustness and sensitivity of retrieved T depends on the used proxy information of abiotic and biotic factors. RS based SIF offers complementary functional vegetation information compared to commonly used vegetation greenness, thus, holds large potential to also advance estimates of T as already demonstrated for GPP. Consequently, several studies already evaluated the sensitivity of SIF for T dynamics and found significant SIF-T relationships (e.g. Lu et al., 2018; Maes et al., 2020; Pagán et al., 2019).

Applying these promising empirical SIF based T approaches across spatial and temporal scales and ecosystems requires consideration of underlying relationships between SIF and T with environmental drivers that could cause a decoupling of SIF and T and can introduce uncertainties in resulting T estimates (Damm et al., 2021). In fact, both canopy SIF and ecosystem T depend differently on several abiotic factors (i.e. net radiation ($R_n$), air temperature ($T_a$), relative humidity (RH)) and biotic factors (i.e. leaf area index (LAI), canopy conductance ($r_s$), net carbon assimilation rate ($A_n$), non-photochemical quenching (NPQ)). Several studies (e.g. Shan et al., 2019; Shan et al. 2021) provide important mechanistic insights by using SIF to represent stomatal conductance in the Penman-Monteith (PM) framework (Monteith, 1965; Penman, 1948) and by evaluating the resulting performance of these SIF based T estimates. Yet other studies suggest multi-sensor RS approaches to account for the complexity of T dynamics (Damm et al., 2021; Jonard et al., 2020). What remains less consolidated yet is a systematic assessment of suited entry points of SIF in T models and of the sensitivity of SIF based T approaches to track T dynamics under changing environmental conditions.

In response to the above stated gap, this study aims to contribute

empirical insights on the sensitivity of different SIF based T approaches for changes in T caused by evolving soil water limitation. We used a comprehensive set of data collected during a field experiment in an agricultural crop. We derived a time series of airborne based SIF along with other abiotic and biotic factors and evaluated several strategies to estimate T, ranging from a simple linear SIF-T model to replacing different PM model parameters with SIF. We evaluated the performance of all approaches by comparing modelled T with independent T estimates derived from land surface temperature (LST) data and in situ sap flow measurements.

## 2. Methods

### 2.1. Test site

Our experiment took place in a maize field located north of the city of Grosseto in Tuscany, Italy (42°50′58.3″N 11°03′48.0″E, Fig. 1a). Irrigation tubes were removed in a small part of the drip-irrigated maize field on 13 June 2019 to gradually reduce soil water availability until 24 June 2019 (water limited area (WL), orange box in Fig. 1b). A second area in close vicinity was selected as reference, representing a structurally and functionally similar maize canopy with a maintained irrigation (well-watered area (WW), blue box in Fig. 1b).

### 2.2. In situ data

In the center of the maize field, we collected air temperature ($T_a$) and relative humidity (RH) few meters above the canopy with a mobile weather station equipped with Vaisala weather sensors. Both $T_a$ and RH were used to parameterize the PM equation to model T. In addition, we installed the FloX field spectrometer system (JB Hyperspectral Devices GmbH, Germany) at the northern border of the water limited maize area to continuously measure dynamics of photosynthetic active radiation (PAR), reflectance and SIF. The FloX was placed 4 m above the canopy, resulting in a footprint size of 1.8 m (considering a field of view of 25°) that allowed capturing approximately 15–17 plants. The FloX system comprises a high-resolution spectrometer (full width half maximum (FWHM) of 0.3 nm between 650 and 800 nm) and a low-resolution spectrometer (FWHM of 1.5 mm between 400 and 950 nm), both measuring radiance and irradiance at high temporal resolution (2-minute interval). We used irradiance measurements of the low-resolution instrument to retrieve incident PAR as spectral integral of measured irradiance between 400 nm and 700 nm.

### 2.3. Sap flow measurements

Sap flow was measured with dual-heater sap flow gauges considering a heat-balance theory (Peressotti and Ham, 1996; Sakuratani, 1981) to represent T ($T_{SAP\text{-}flow}$). We installed ten sap flow gauges in both the WW and WL maize areas and measured sap flow every 15 min in g $hr^{-1}$. The unit of provided sap flow data was converted from g $hr^{-1}$ per plant to mm $hr^{-1}$ to compare the measured sap flow with modelled T that are expressed in mm $hr^1$. Therefore, we multiplied sap flow (g $hr^{-1}$) with the number of maize plants per $m^2$ and divided by 1000 to convert g $m^{-2}$ $hr^{-1}$ in mm $hr^{-1}$. The plant density differed with 6.92 plants per $m^2$ in the WW area and 7.03 plants per $m^2$ in the WL area.

### 2.4. Airborne data

A total of 42 airborne data sets were acquired between the 16 and 24 of June 2019. The data acquisition time in the morning was between 10:11 and 11:41 local time (l.t.), and in the afternoon between 13:15 and 14:37 l.t. (cf. Damm et al., 2022 for details). Data used in this study stem from two different airborne sensors including the fluorescence spectrometer HyPlant (Rascher et al., 2015) and the thermal imager TASI (Hanuš et al., 2016).

HyPlant is an imaging spectrometer designed to measure SIF in addition to common RS vegetation information. The system consists of two modules, with the DUAL module covering the optical wavelength range between 380 and 2500 nm in high spectral resolution (i.e. FWHM between 3.65 nm and 10.55 nm) and the FLUO module covering the wavelength range between 670 and 780 nm with a FWHM of 0.28 nm (Rascher et al., 2015; Siegmann et al., 2019). HyPlant data were acquired with a spatial resolution of 2.3 m and used to calculate different vegetation indices and to retrieve SIF at 760 nm via an adapted version of the Spectral Fitting technique (Cogliati et al., 2015; Meroni et al., 2010). Details about the sensor and processing scheme can be found in Siegmann et al. (2019).

On the same aircraft, the TASI-600 (Itres) thermal radiometer was installed to acquire thermal radiation for the retrieval of LST. The TASI push broom line scanner measures longwave radiation between 8000 nm and 11500 nm with a spectral resolution of 110 nm. Data were acquired in 1.8 m spatial resolution and underwent a standard processing workflow (cf. Hanuš et al. (2016) and https://olc.czechglobe.cz/en/processing/tasi-data-processing/ for further details about the data processing).

### 2.5. Standard T approaches ($T_{PM}$, $T_{BB}$)

The PM equation (Monteith, 1965; Penman, 1948) was selected as standard method in our study to estimate T (Eq. (1)). The PM equation is the foundation of the official Food and Agriculture Organization of the United Nations (FAO) evapotranspiration (ET) approach and has been widely applied to estimate ET for different ecosystems from regional to global scale (Allen et al., 1998; Langensiepen et al., 2009). It must be noted that the PM equation typically provides estimates of ET, comprising the sub-components T of plants and evaporation (E) of soil and vegetated surfaces. Given the dense canopy, the lack of in situ measurements of plant and soil evaporation, and the conditions with a rather dry canopy and soil, we can assume that plant and soil E represented only a small percentage of the total canopy evapotranspiration (ET). We thus consider the resulting PM based ET estimates as T rather than ET. According to the FAO adapted PM approach by Allen et al. (1998), T can be expressed as a function of energy constraints, atmospheric parameters and a plant-specific constraint as:

$$T = \frac{\Delta(R_n - G) + \rho_a C_p \left(\frac{e_s - e_a}{r_a}\right)}{\Delta + \gamma\left(1 + \frac{r_s}{r_a}\right)} \quad (1)$$

Here Δ is the slope of the vapor pressure curve in kPa $^oC^{-1}$, $R_n$ and G represent net radiation and soil heat flux density in W $m^{-2}$, respectively, $\rho_a$ is the air density in kg $m^{-3}$, $C_p$ represents the specific heat of the air in J $kg^{-1}$ $^oC^{-1}$, ($e_s$ – $e_a$) represents the saturation vapor pressure deficit or VPD in k Pa with $e_s$ as the saturation vapor pressure and $e_a$ as the actual vapor pressure, $r_a$ and $r_s$ are the aerodynamic and surface resistance in s $m^{-1}$, respectively, and γ is the psychrometric constant in k Pa $^oC^{-1}$. We refer to Allen et al. (1998) for the formulas to calculate Δ, $\rho_a$, $C_p$, $e_s$, and $e_a$.

$R_n$ is a function of net short-wave (*nSW*) and long-wave (*nLW*) radiation or their sub-components incoming short-wave ($SW_{in}$), incoming long-wave ($LW_{in}$), outgoing short-wave ($SW_{out}$), and outgoing long-wave radiation ($LW_{out}$) (Allen et al., 1998; Liang, 2004; Wang and Liang, 2009), and can be expressed as:

$$R_n = nSW + nLW = SW_{in} - SW_{out} + LW_{in} - LW_{out} \quad (2)$$

*nSW* can be considered as function of solar radiation ($R_S$) and surface albedo ($\alpha$) (Allen et al., 1998; Campbell and Norman, 1998; Liang, 2004) and can be expressed as:

$$nSW = R_s(1 - \alpha) \quad (3)$$

Based on the Stefan-Boltzmann law of radiation, $LW_{out}$ and $LW_{in}$ are a

**Table 1**
Parameterization of the standard and the five experimental approaches to estimate transpiration (T). For the calculation of individual parameters we refer to the individual equations shown in the text.

| Parameter | $T_{PM}$ | $T_{BB}$ | $T_{SIF4T}$ | $T_{SIF4Rn}$ | $T_{SIF4rs}$ | $T_{SIF4LAI}$ | $T_{SIF4An}$ |
|---|---|---|---|---|---|---|---|
| Energy constraints | | | | | | | |
| $R_n$ | In situ/airborne | | SIF | SIF | In situ/airborne | | |
| G | $0.1R_n$ | | SIF | SIF | $0.1R_n$ | | |
| Atmospheric constraints | | | | | | | |
| Δ | In situ ($T_a$) | | SIF | In situ ($T_a$) | | | |
| $\rho_a$ | Constant: 101.26 | | SIF | Constant: 101.26 | | | |
| $C_p$ | In situ ($T_a$) | | SIF | In situ ($T_a$) | | | |
| $e_s$- $e_a$ | In situ ($T_a$) | | SIF | In situ ($T_a$) | | | |
| $r_a$ | Constant: 38.63 (wind speed 1.5 m $s^{-1}$, canopy height 2 m) | | SIF | Constant: 38.63 (wind speed 1.5 m/s, canopy height 2 m) | | | |
| γ | In situ (P) | | SIF | In situ (P) | | | |
| Biological control PM ($r_l$) | | | | | | | |
| $r_l$ | $f(R_n)$ | – | SIF | $f(R_n)$ | SIF | $f(R_n)$ | $f(R_n)$ |
| Biological control BB ($1/r_l$ or $g_s$) | | | | | | | |
| $a_1$ | – | 8.0 | | – | | | 8.0 |
| $A_n$ | – | $R_n/0.0431$ | | – | | | SIF |
| $c_s$ | – | 470 | | – | | | 470 |
| Γ | – | 70 | | – | | | 70 |
| $D_s$ | – | In situ ($T_a$) | | – | | | In situ ($T_a$) |
| $D_o$ | – | 0.167 | | – | | | 0.167 |
| Scaling of $r_l$ to $r_s$ | | | | | | | |
| LAI | HyPlant (SR) | | SIF | HyPlant (SR) | SIF | SIF | HyPlant (SR) |

function of surface and air emissivity ($\varepsilon_s$ and $\varepsilon_a$), surface and air temperature ($T_s$ and $T_a$), and the Stefan-Boltzmann constant ($\sigma$) (Allen et al., 1998; Campbell and Norman, 1998; Wang and Liang, 2009) and can be expressed as:

$$LW_{out} = \varepsilon_s \sigma (T_s)^4 \quad (4)$$

$$LW_{in} = \varepsilon_a \sigma (T_a)^4 \quad (5)$$

Because we do not have measurements of all required data (e.g. emissivity) and need $T_S$ as independent information to validate modelled T, we applied a more simplified approach. It must be noted that there are established RS products available to parameterize Eq. (2) but they are only available at a rather coarse spatial resolution not appropriate for our study focusing on data with a 2.3 m spatial resolution. The implemented simplified approach particularly considered the good agreement between $R_n$ and absorbed photosynthetic active radiation (APAR) found in previous studies (Oliphant et al., 2006; Green et al., 1995). The study by Oliphant et al. (2006) showed significant similarity between $R_n$ and APAR over a forest canopy. Another study showed that net PAR (sum of incoming and outgoing PAR which equals APAR (Toll et al., 1994)) showed similarity to $R_n$ dynamics over a single tree canopy (Green et al., 1995). We therefore expressed $R_n$ as a function of APAR as:

$$R_n = APAR \times 1.8 = (PAR \times 0.0036 \times (NDVI \times 1.235 - 0.211)) \times 1.8 \quad (6)$$

APAR was calculated as a product of PAR and the fraction of absorbed photosynthetic active radiation (fAPAR). Local FloX data were used to obtain PAR measurements in W $m^{-2}$, the unit conversion in MJ $m^{-2}$ $hr^{-1}$ was achieved via the factor 0.0036. fAPAR was derived following Zhang et al. (2015) as a linear function of the normalized difference vegetation index (NDVI). The resulting APAR was then scaled by the empirically derived factor of 1.8 (cf. Appendix-A for a description of the empirical scaling approach) to approximate $R_n$ per pixel.

A common approach to estimate G according to Allen (2005) is:

$$G = G_{z_s} + C_s \int_0^{z_s} \frac{\partial T_s}{\partial t} d_{z_s} \quad (7)$$

Where $C_s$ (in m) is the sum of the shaded soil fraction that is either wet ($C_{sW}$) or dry ($C_{sD}$), and $G_{z_s}$ is the soil heat flux in W $m^{-2}$ at a shallow depth ($z_s$) (e.g. 0.01 m). As we did not measure $G_{z_s}$ and temperature changes between soil surface and $z_s$ over time ($\frac{\partial T_s}{\partial t} dz_s$), we applied a more simplified G estimation proposed for short vegetation by Allen (2005):

$$G = 0.4 e^{-0.5LAI} R_n \quad (8)$$

LAI represents the leaf area index in $m^2$ $m^{-2}$. Given LAI values ranging between 2.8 and 5.8 in our experimental fields, we again simplified the calculation of $G$ by assuming $G = 0.1R_n$.

$r_s$ was calculated according to Allen (2005) as:

$$r_s = \frac{r_l}{LAI \times 0.5} \quad (9)$$

$r_l$ represents the leaf resistance. According to Gong et al. (2017), $r_l$ can be approximated as a function of $R_n$ as:

$$r_l = 23.21 exp\left(\frac{1021.06}{R_n + 365.71}\right) \quad (10)$$

We obtained all relevant parameters from in situ observations ($T_a$, RH, $R_n$) and HyPlant airborne data (cf. Table 1) to calculate a standard T time series (i.e. $T_{PM}$).

As an alternative to approximate the biological constraint on T (i.e. $r_s$), we used the Ball-Berry-Leuning (BBL) approach after (Ball et al., 1987) and (Leuning, 1995) to estimate leaf resistance and subsequently $r_s$ as:

$$\frac{1}{r_l} = g_s = g_0 + \frac{a_1 A_n}{(c_s - \Gamma)\left(1 + \frac{D_s}{D_0}\right)} \quad (11)$$

$g_s$ is the stomatal conductance in mol $CO_2$ $m^{-2}$ $s^{-1}$, $g_0$ is the stomatal conductance at the light compensation point in mol $CO_2$ $m^{-2}$ $s^{-1}$, $A_n$ represents the net leaf $CO_2$ assimilation rate in mol $CO_2$ $m^{-2}$ $s^{-1}$, $c_s$ is the leaf surface $CO_2$ partial pressures in mol $CO_2$ mol $air^{-1}$, $D_s$ represents the water vapor partial pressure deficit at the leaf surface, Γ is the $CO_2$ compensation point, and $a_1$ and $D_0$ are two empirical coefficients. For our experiment, we used the standard parameters suggested. The combination of the BBL model with the PM equation resulted in a second standard T time series (i.e. $T_{BB}$).

For the spatial representation of LAI, we used data from the HyPlant FLUO module to retrieve the simple ratio (SR) vegetation index and eventually applied the SR as a proxy for the LAI. In situ LAI measurements made with a LAI-2000 (LICOR Inc., Lincoln, NE, USA) were used to derive a linear empirical model between the SR and LAI ($LAI = 0.1787 \times SR + 0.9297$), and estimate LAI per pixel. It must be noted that vegetation indices can be subject to illumination changes (Damm et al., 2015b), causing an unrealistic daily variability. This would mean that LAI and fAPAR are different in the morning and afternoon. We

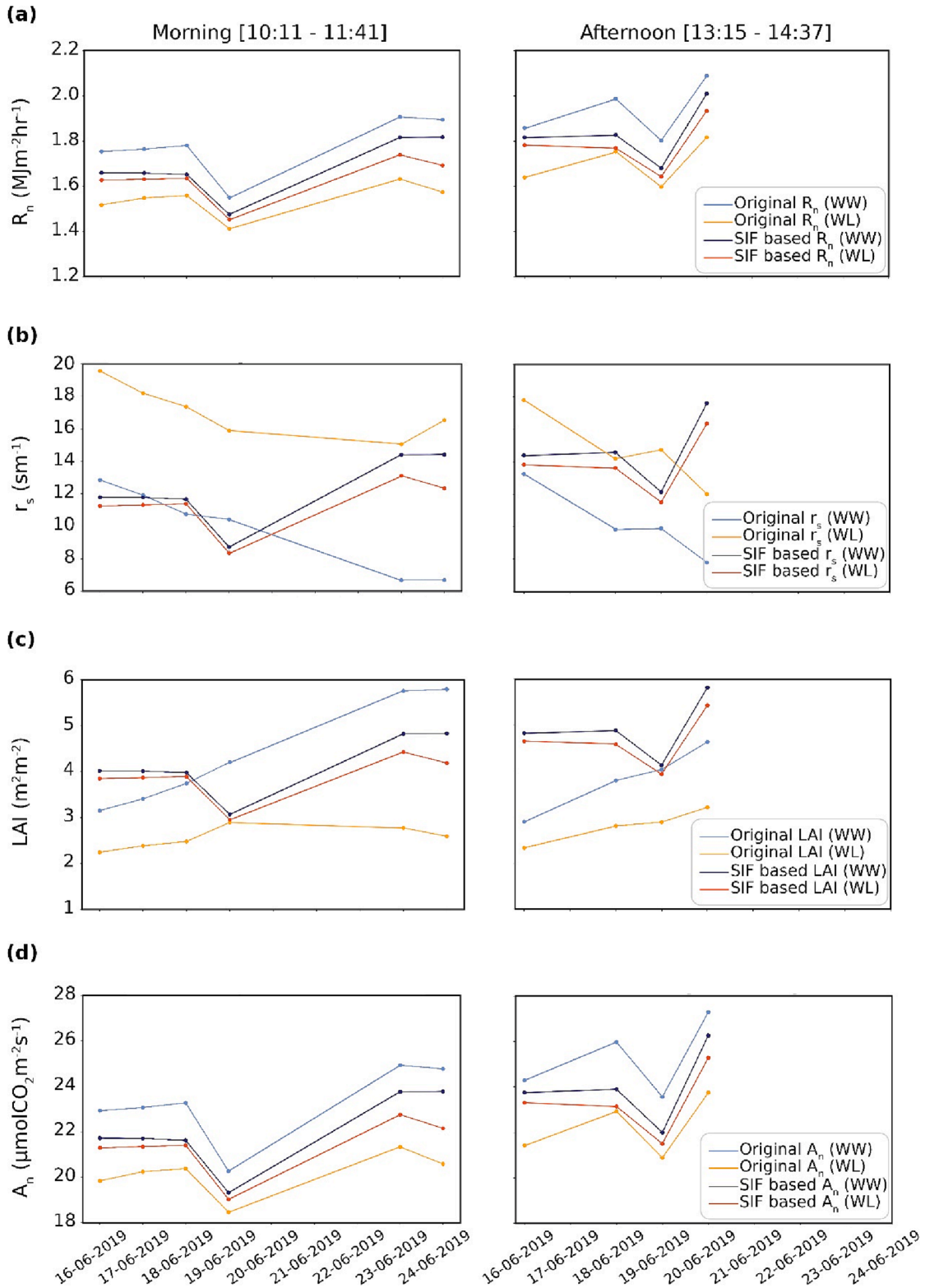


**Fig. 2.** Time series of original and sun-induced chlorophyll fluorescence (SIF)-based estimates of (a) net radiation ($R_n$, MJ m$^{-2}$ hr$^{-1}$), (b) surface resistance ($r_s$, s m$^{-1}$), (c) leaf area index (LAI, m$^2$ m$^{-2}$), and (d) net leaf $CO_2$ assimilation rate ($A_n$, µmol $CO_2$ m$^{-2}$ s$^{-1}$) for the well-watered (WW) and water-limited (WL) maize areas. The data has been separated for morning and afternoon data acquisition.

compensated this by interpolating afternoon values using nearest morning values.

### 2.6. Strategies to integrate SIF in T modelling

We evaluated five strategies, or experiments, to ingest SIF in PM- and BBL-based T modelling schemes. Investigated strategies are at different levels of approximation and include a replacement of T with SIF

(experiment 1, rough approximation), a replacement of two vegetation related drivers of T as embedded in the PM approach with SIF, i.e. $R_n$, $r_s$, (experiments 2–3, medium approximation), and a replacement of two vegetation related drivers used to calculate $r_s$ in the PM and the BBL approach, i.e. LAI and $A_n$ respectively (experiments 4–5, detailed approximation). Experiment one follows ideas as found in literature (Lu et al., 2018). The base of experiment two is a partial relation between $R_n$ with SIF as outlined below, while experiment three to five was inspired by the work of Shan et al. (2019, 2021) .

It is essential to note that physical units and value ranges of SIF, T and the evaluated model parameters differ. We therefore applied a unity-based normalization to SIF (SIFn) considering the minimum (min) and maximum (max) SIF values of the entire time series of the WL and WW area:

$$SIF_n = \frac{(SIF - SIF_{min})}{(SIF_{max} - SIF_{min})} \quad (12)$$

Afterwards, we re-scaled $SIF_n$ to the value range of the target variables (V) using their respective value range (via min and max values) considering the entire time series of the WL and WW area, resulting in $V^{SIF}$:

$$V^{SIF} = SIF_n \times (V_{max} - V_{min}) + V_{min} \quad (13)$$

Here, V represents the target variables T, $R_n$, $r_s$, LAI and $A_n$, the outcomes are illustrated in Fig. 2. It must be noted that the applied unity-based normalization assumes linearity between SIF and the target variables. This is a simplification of e.g. the well-known hyperbolic relationship between $A_n$ and SIF (i.e. Damm et al., 2015a; Gu et al., 2019; Liu et al., 2022), but justified by the small variable range within our experiment and the lack of more detailed physiological data to uncover more complex relationships.

#### 2.6.1. Experiment one: SIF to approximate T (SIF4T)

For experiment one, we evaluate if SIF can be used as a single proxy for T, thus, representing all constraints on T including atmospheric, energy and biologic controls. Experiment one (SIF4T) is justified by recent studies indicating that T could be solely approximated by SIF (Lu et al., 2018). We applied Eqs. (12) and (13) to scale SIF and obtained $T_{SIF4T}$ that corresponds to the value range of T calculated with the standard approach (i.e. $T_{PM}$) for the entire time series of the maize field.

#### 2.6.2. Experiment two: SIF to approximate $R_n$ ($SIF4R_n$)

For experiment two ($SIF4R_n$), we evaluate if SIF can be used to replace $R_n$ in the PM equation. Replacing $R_n$ with SIF could be justified by the mechanistic relation of SIF with APAR (Damm et al., 2015a; Mohammed et al., 2019). It must be mentioned that this SIF-based approach represents only the PAR region between 400 nm and 700 nm, while $R_n$ considers both short wave and long wave radiation of the electromagnetic spectrum, but we found a good agreement between APAR and $R_n$ (cf. Appendix-A). The scaling of SIF (Eqs. (12) and (13)) resulted in $R_n^{SIF}$, with a value range corresponding to $R_n$ from the entire time series of the maize field (c.f. Fig. 2a). $R_n^{SIF}$ was then ingested in the PM modeling scheme (Eq. (2)) for T estimates ($T_{SIF4Rn}$).

#### 2.6.3. Experiment three: SIF to approximate $r_s$ ($SIF4r_s$)

We evaluate in our third experiment ($SIF4r_s$) if SIF can be used to replace $r_s$ in the PM equation (Eq. (2)). Mechanistically, $r_s$ should be related to photosynthesis because it is driven by the photosynthetic $CO_2$ demand. This suggests that SIF may also have a correlation with $r_s$ through a complex set of physical and biophysical mechanisms. In fact, recent studies used $r_s$ as an entry point of SIF for T estimates (Shan et al., 2019; Shan et al. 2021). The scaling of SIF (Eqs. (12) and (13)) resulted in $r_s^{SIF}$, with a value range corresponding to $r_s$ (c.f. Fig. 2b) as used in the standard approach $T_{PM}$ for the entire time series of the maize field. $r_s^{SIF}$ was then ingested in the PM modeling scheme (Eq. (2)) to estimate T ($T_{SIF4rs}$).

#### 2.6.4. Experiment four: SIF to approximate LAI (SIF4LAI)

According to Eq. (9), $r_s$ can be approximated as a function of $r_l$ and LAI. Since canopy SIF is largely dependent on LAI (Damm et al., 2021), we defined a fourth experiment (SIF4LAI) and evaluated if SIF can be used to replace LAI in the PM model, thus indirectly modifying $r_s$. $LAI^{SIF}$ was obtained using Eqs. (12) and (13) to have a value range corresponding to the LAI used in the standard approach $T_{PM}$ for the entire time series of the maize field (c.f. Fig. 2c). $LAI^{SIF}$ was then ingested in the PM modeling scheme (Eq. (9)) to estimate T ($T_{SIF4LAI}$).

#### 2.6.5. Experiment five: SIF to approximate $a_n$ (SIF4An)

A last experiment made use of the BBL model that offers with its parameter $A_n$ another interesting entry point of SIF for the modelling of T. Since SIF is known to be highly correlated to $A_n$ or GPP (e.g. Dechant et al., 2020; Guanter et al., 2014; Wieneke et al., 2016), we defined the experiment $SIF4A_n$ and replaced $A_n$ in the BBL equation (Eq. (11)) with SIF. This allows to modify estimates of $r_l$ (Eq. (10)), later $r_s$ (Eq. (9)) and eventually T (Eq. (2)) ($T_{SIF4An}$). Since we did not have $A_n$ observations, we scaled the value range of SIF (Eqs. (12) and (13)) to obtain $A_n^{SIF}$ matching typical values of $A_n$ in maize canopies (0–25 μmol $CO_2$ $m^{-2}$ $s^{-1}$) (c.f. Fig. 2d) (Peng et al., 2011; Peng and Gitelson, 2011).

### 2.7. Normalization and evaluation of modelling strategies

#### 2.7.1. Quantification of water limitation on T

After calculating T with the two standard ($T^S$) and five experimental approaches ($T^E$), we normalized the $T^S$ and $T^E$ time series of the WL area ($T_{WL}^{S,E}$) using the time series of the WW area ($T_{WW}^{S,E}$) as reference:

$$nT_{WL,WW}^{S,E} = \left(\frac{T_{WL}^{S,E} - T_{WW}^{S,E}}{T_{WW}^{S,E}}\right) \times 100 \quad (14)$$

The resulting $nT_{WL,WW}^{S,E}$ time series represents the percentage difference of modelled T between the WL and WW area over time and, thus, allows quantifying the effect of applied water limitation on T. The normalization was important to compensate variations caused by combined effects of illumination and canopy structure, atmospheric disturbances or other observational artefacts.

#### 2.7.2. Relative sensitivity of SIF informed T modelling for T dynamics

Calculated $nT_{WL,WW}^{S,E}$ time series were used to calculate the difference between $nT_{WL,WW}^{E}$ (i.e. the five SIF experiments) and $nT_{WL,WW}^{S}$ (i.e. the two standard approaches $T_{PM}$, $T_{BB}$) as:

$$r\Delta T_{EXP} = \left(nT_{WL,WW}^{E} - nT_{WL,WW}^{S}\right) \quad (15)$$

Resulting $r\Delta T_{EXP}$ represent the relative (since it is related to a standard approach, not an absolute reference) sensitivity of SIF informed T modelling for changes in T due to soil water limitation. The use of $T_{PM}$, $T_{BB}$ as standard is justified by their widespread implementation, e.g. by the FAO.

#### 2.7.3. Absolute sensitivity of standard and SIF informed T modelling for T dynamics

We calculated the absolute sensitivity of SIF informed modelling for T dynamics to better interpret derived relative sensitivities ($r\Delta T_{EXP}$) and evaluate whether they result in an improved or reduced T modelling capacity. In absence of spatially explicit reference T measurements (note that sap flow data are point measurements), we used LST as proxy for reference T. We normalized the LST time series considering the value ranges of $T_{PM}$ of the WW and WL area using Eqs. (12) and (13) to derive $T^{LST}$. We then calculated the relative difference of $T^{LST}$ between the WL and WW areas ($nT_{WL,WW}^{LST}$) using Eq. (14). The absolute sensitivity of the

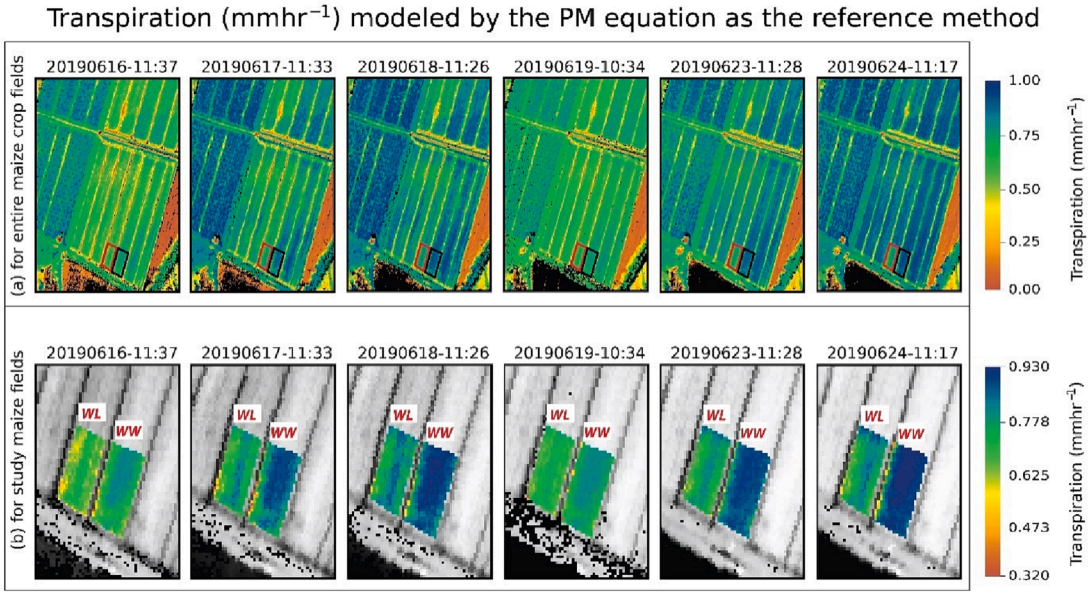


**Fig. 3.** Spatiotemporal changes in modeled transpiration by the Penman-Monteith (PM) equation ($T_{PM}$) for (a) the entire maize field. The well-watered (WW) canopy area is marked in red, the water-limited (WL) in black. (b) A detailed representation of $T_{PM}$ changes for the WW and WL area, both are colored and T of the remaining area is show in gray values. (For interpretation of the references to color in this figure legend, the reader is referred to the web version of this article.)

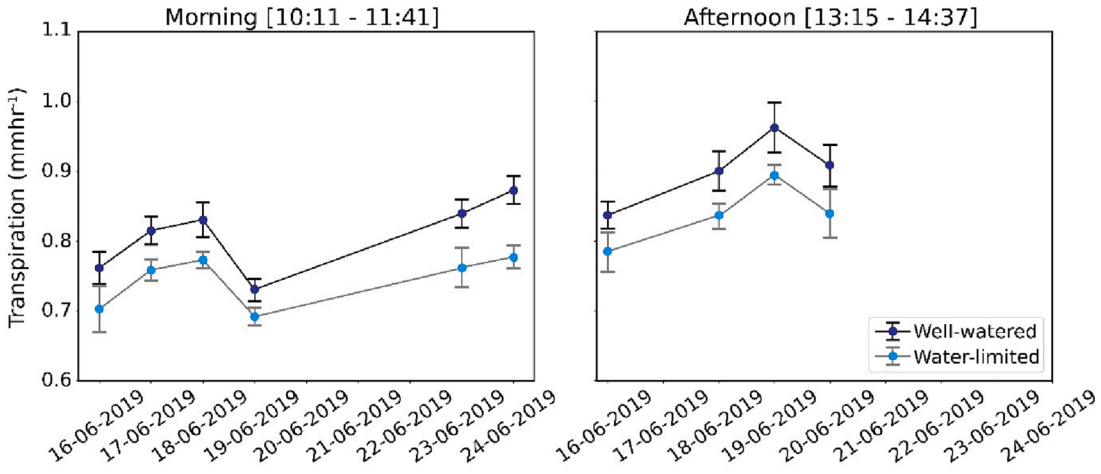


**Fig. 4.** Changes in average transpiration (T) (mm hr$^{-1}$) for the well-watered (WW) and water-limited (WL) maize area in the morning (left) and afternoon (right). Shown values represent the average for all observations per day and all approaches, i.e. the two standard ($T_{PM}$ & $T_{BB}$) and the five sun-induced chlorophyll fluorescence (SIF) based approaches ($T_{SIF4T}$, $T_{SIF4Rn}$, $T_{SIF4rs}$, $T_{SIF4LAI}$, & $T_{SIF4An}$). Error bars represent the standard deviation for each set of T estimates per day.

two standard approaches and five SIF experiments was then quantified as:

$$a\Delta T_{STD,EXP} = \left(nT^{S,E}_{WL,WW} - nT^{LST}_{WL,WW}\right) \quad (16)$$

It must be noted that we assumed an inverse relationship between LST and T, as a reduction in T causes an increase in LST due to reduced evapotranspirative cooling.

## 3. Results

### 3.1. Spatio-temporal transpiration dynamics

Six spatial datasets out of 42 have been selected to visually represent the spatial changes in $T_{PM}$ during the study period for both treatments, i.e. WW and WL (Fig. 3a). An increasing difference of $T_{PM}$ between the WW and WL area is visible (Fig. 3b). At the beginning of the experiment, $T_{PM}$ was higher in the WW field (0.75 mm hr$^{-1}$) compared to the WL field (0.66 mm hr$^{-1}$). At the end of the experiment on 24 June, $T_{PM}$ of the WW field increased to 0.89 mm hr$^{-1}$, while $T_{PM}$ of the WL area showed a reduced increase to 0.76 mm hr$^{-1}$. This resulted in an increased difference between the WW and WL area of 0.13 mm hr$^{-1}$ compared to the start of the experiment on 16 June (0.09 mm hr$^{-1}$). Results of both standard approaches and the five SIF experiments are similar, detailed statistics are provided in Table A1.

A time series representing the average of T changes for both standard and the five SIF approaches for all observations per day is shown in Fig. 4. Results indicate a consistent increase of T in both canopy areas (WW, WL) in the morning. One exception is 19 June, where data was acquired one hour earlier (10:11–10:34) compared to the other days (11:09–11:41). It can be observed that T between the WL and the WW area increasingly differed after 19 June, with T of the WL areas showing a less steep increase over the duration of the experiment (Fig. 4 left). For the afternoon, T in both the WW and WL area also increased, while the large increase on 19 June was related to an earlier observation time at

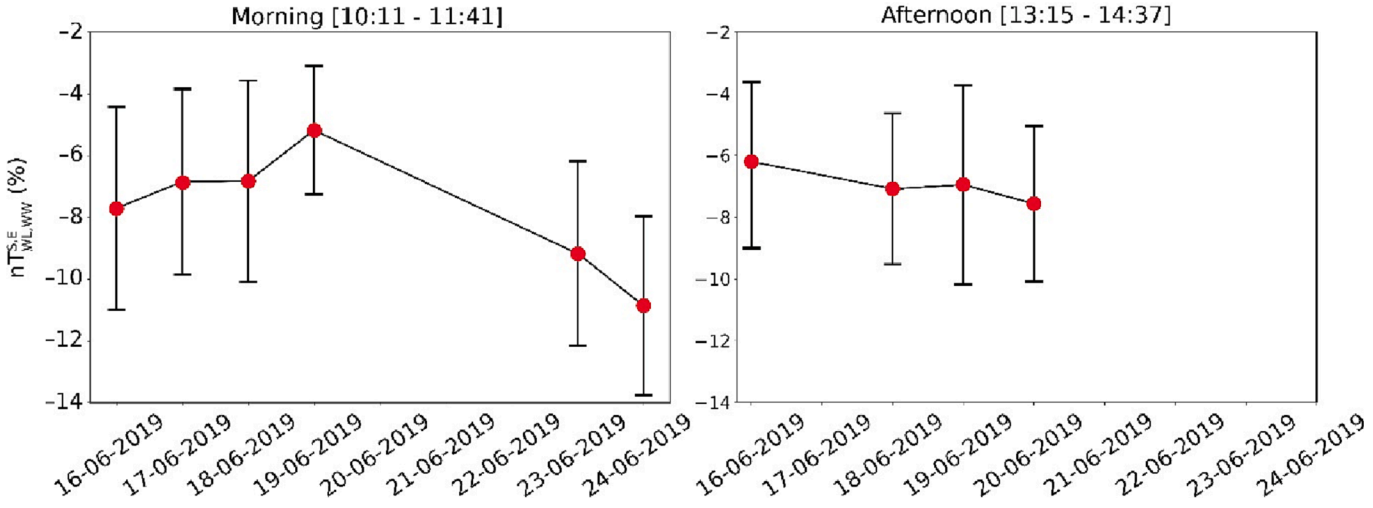


**Fig. 5.** Normalized difference ($nT^{S,E}_{WL,WW}$) of transpiration (T) derived from the standard ($T^S$) and the sun-induced chlorophyll fluorescence (SIF) based approaches ($T^E$) between the water-limited (WL) and the well-watered (WW) canopy area for morning (left) and afternoon (right). Shown values represent the average for all T approaches for all observations per day, the error bars represent the related standard deviation.

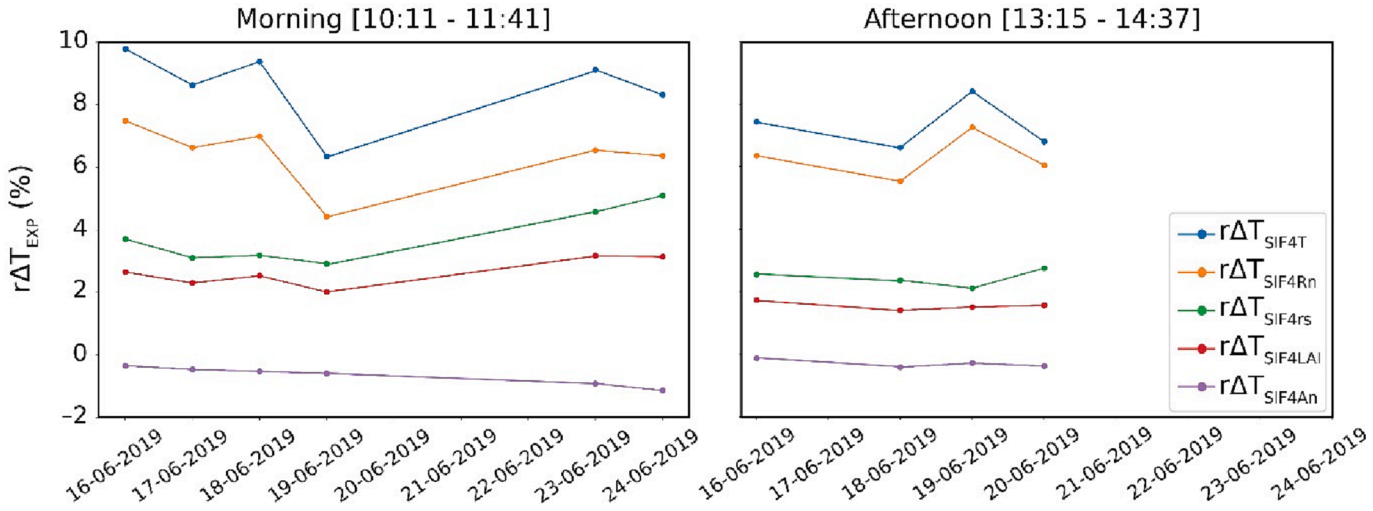


**Fig. 6.** Relative sensitivity ($r\Delta T_{EXP}$) of five sun-induced chlorophyll fluorescence (SIF) based experimental transpiration (T) estimates ($T_{SIF4T}$, $T_{SIF4Rn}$, $T_{SIF4rs}$, $T_{SIF4LAI}$, and $T_{SIF4An}$) to track changes in T caused by increasing soil water limitation. Five SIF-based T experiments were compared against two standard T estimates ($T_{PM}$ and $T_{BB}$).

solar noon (13:15–13:38) compared to the other days (14:11–14:37). The difference between T from both areas did not change in the afternoon (Fig. 4 right).

### 3.2. Impact of soil water limitation on transpiration

The above assessment of T dynamics during the experiment indicated clear differences between the WW and the WL canopy areas, particularly at the end of the experiment. The pronounced variability in T across days due to differing acquisition times (Fig. 4), however, complicated a more thorough assessment. We therefore normalized all T time series of the WL area considering the WW area ($nT^{S,E}_{WL,WW}$), results are shown in Fig. 5. Besides the generally lower T values of the WL area, results indicate an increasing difference of T between the WL and the WW area from –7.0 % to –10.87 % (morning) and from –6.5 % to –7.56 % (afternoon). The exceptional $nT^{S,E}_{WL,WW}$ value for 19 June (–5.0 %) is caused by an approximately one hour earlier observation time compared to the other days (Fig. 5).

### 3.3. Relative effect of SIF in T modelling

SIF was differently ingested in T modeling approaches. Here we quantify the relative effect of using SIF to approximate different model parameters on T ($r\Delta T_{EXP}$) as difference between the normalized T of the SIF experiments ($nT^{E}_{WL,WW}$) and the standard approaches ($nT^{S}_{WL,WW}$). Results indicate that $T_{SIF4An}$ differed less (–1.1 to –0.1 %) from $T_{PM}$ throughout the experimental period, followed by $T_{SIF4LAI}$ (1.4 to 3.2 %), $T_{SIF4rs}$ (2.1 to 5.1 %), $T_{SIF4Rn}$ (4.4to 7.5 %), and $T_{SIF4T}$ differing the most (6.3 to 9.8%) (Fig. 6).

The root mean square error (RMSE) and coefficient of determination ($r^2$) considering morning and afternoon data confirmed the relatively small impact of SIF on T modelling when replacing $A_n$ ($T_{SIF4An}$: RMSE = 0.58 %, $r^2$ = 0.98), LAI ($T_{SIF4LAI}$: RMSE = 2.19 %, $r^2$ = 0.94) and $r_s$ ($T_{SIF4rs}$: RMSE = 3.23 %, $r^2$ = 0.84). In contrast, replacing $R_n$ with SIF and approximating T with SIF showed highest deviations (for $T_{SIF4Rn}$: RMSE = 6.23 %, $r^2$ = 0.46; for $T_{SIF4T}$: RMSE = 7.97 %, $r^2$ = 0.21) (Fig. 7).

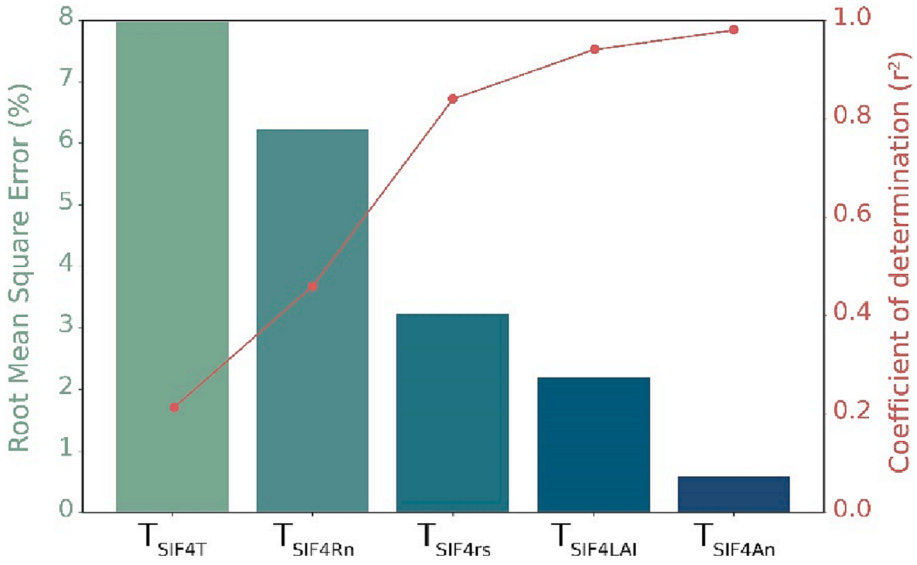


**Fig. 7.** Effect of using sun-induced chlorophyll fluorescence (SIF) in transpiration (T) modeling quantified by the root mean square error (RMSE) and coefficient of determination ($r^2$). Five SIF-based approaches were considered: $T_{SIF4T}$, $T_{SIF4Rn}$, $T_{SIF4rs}$, $T_{SIF4LAI}$, and $T_{SIF4An}$. RMSE and $r^2$ relate the normalized difference of standard T approaches ($nT^{S}_{WL,WW}$) with the normalized difference of the SIF experimental approaches ($nT^{E}_{WL,WW}$). RMSE and $r^2$ were calculated without separating morning and afternoon time series.

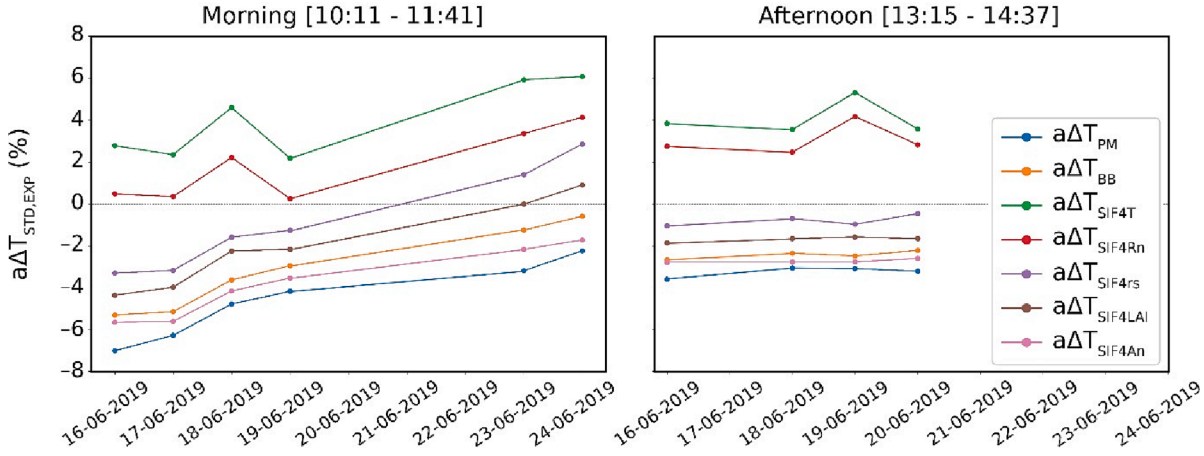


**Fig. 8.** Absolute difference ($a\Delta T_{STD,EXP}$) between a land surface temperature (LST) based transpiration (T) estimate and the five sun-induced fluorescence (SIF) based and two standard T approaches ($T_{PM}$ and $T_{BB}$).

### 3.4. Absolute effect of SIF in T modelling using LST

The above evaluated relative effect of using SIF in T modelling cannot reveal if the use of SIF results in improved T estimates or not. An absolute T reference is needed for such an assessment. As no direct spatial T reference data was available, we used an LST based approximation of T. The absolute effect of using SIF was quantified as difference between the normalized T time series $nT^{S,E}_{WL,WW}$ (considering both reference and the five approaches) and the normalized LST based T estimate ($nT^{LST}_{WL,WW}$). The resulting $a\Delta T_{STD,EXP}$ indicates that among all SIF-based T approaches, $T_{SIF4rs}$ showed the closest agreement with LST based T dynamics (Fig. 8), related statistical measures confirm this (i.e. RMSE of 1.97 %, $r^2$ of 0.32, Fig. 9). $T_{SIF4An}$ and $T_{SIF4T}$ showed larger deviations (RMSE of 3.64 % and $r^2$ 0.58, RMSE of 4.14 %, $r^2$ of 0.44, Fig. 9). The results also indicate that replacing $r_s$, LAI, and $R_n$ with SIF can outperform both standard approaches ($T_{PM}$, $T_{BB}$) in terms of RMSE, while only replacing LAI and $A_n$ with SIF results in a higher $r^2$ compared to both standard approaches.

### 3.5. In situ based assessment of SIF based T modelling approaches

Sap flow data were used as independent evaluation of T dynamics derived from the standard and SIF-based T approaches. The comparison indicates that all implemented RS-based T modelling approaches overestimate T by 0.28 mm $hr^{-1}$ for the WW and 0.27 mm $hr^{-1}$ for the WL area (Fig. 10). The temporal behavior of $T_{SAP\text{-}flow}$ and the evaluated standard and SIF-based T approaches are comparable for the WW and WL area in the morning (i.e. $r^2 = 0.76$ for WW and WL). In the afternoon, the temporal agreement between $T_{SAP\text{-}flow}$ and the RS-based T estimates are less consistent, resulting for the WW area in an $r^2$ of 0.20 and for the WL area in an $r^2$ of 0.02.

A more detailed evaluation of relationships between $T_{SAP\text{-}flow}$ and the individual standard and SIF-based T approaches is shown in Table 2. This assessment indicates that $T_{SIF4rs}$ shows the largest agreement with $T_{SAP\text{-}flow}$ ($r^2$ between 0.19 and 0.90, RMSE between 0.36 and 0.21), while $T_{SIF4T}$ agrees least ($r^2$ between 0.22 and 0.48, RMSE between 0.38 and 0.21).

## 4. Discussion

### 4.1. Considerations on SIF-based T modelling

This study systematically investigated experimental strategies to ingest SIF in T modelling approaches. Both evaluated standard approaches and the five SIF-based derivatives indicate a reduced T with

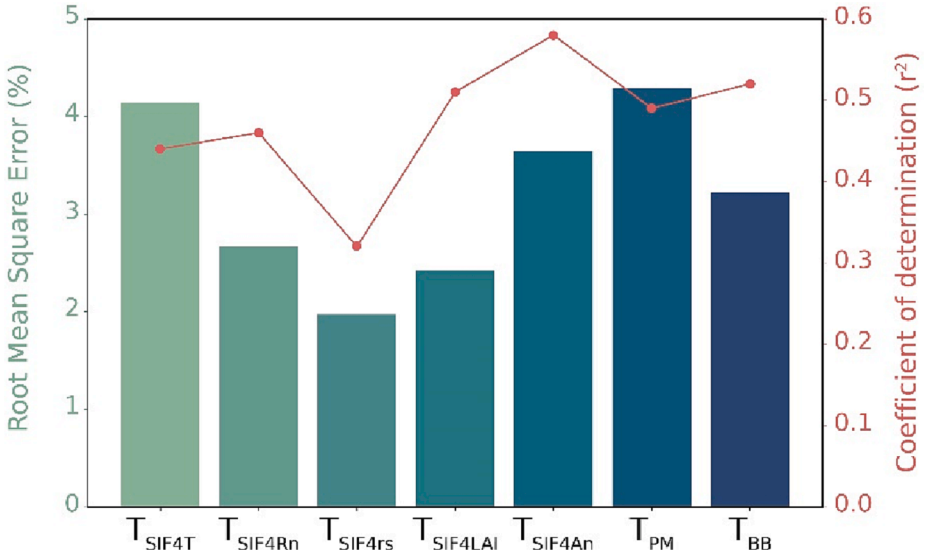


**Fig. 9.** Summary statistics (root mean square error (RMSE) and coefficient of determination ($r^2$)) describing the absolute difference between a land surface temperature (LST) based transpiration (T) estimate and the five sun-induced chlorophyll fluorescence (SIF) based and two standard T approaches ($T_{PM}$ and $T_{BB}$). RMSE and $r^2$ were calculated without separating morning and afternoon time series.

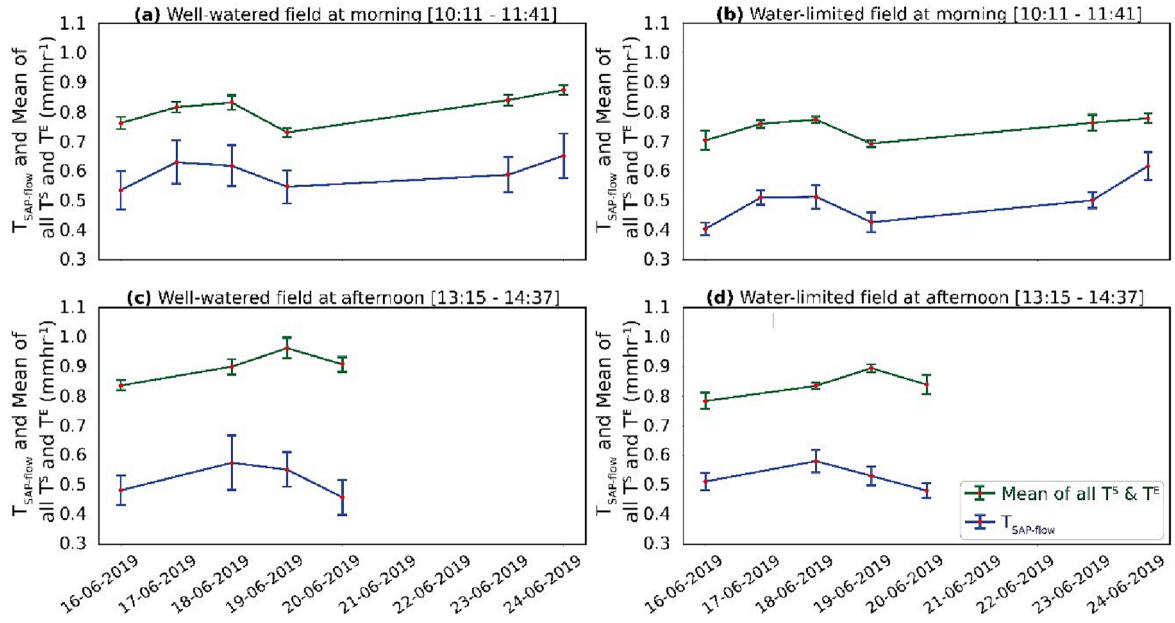


**Fig. 10.** Comparison between the average of transpiration (T) modelled with the standard approaches ($T^S$) and sun-induced chlorophyll fluorescence (SIF) based approaches ($T^E$) and derived from sap flow measurements ($T_{SAP\text{-}flow}$) for all methods per day. WW represents the well-watered canopy area, WL the water limited one. The error bars represent the standard deviation.

**Table 2**
The coefficient of determination ($r^2$) and root mean square error (RMSE) between sap flow-based transpiration (T) ($T_{SAP\text{-}flow}$) and two standard approaches ($T_{PM}$ and $T_{BB}$) and five sun-induced chlorophyll fluorescence (SIF) based approaches ($T_{SIF4T}$, $T_{SIF4Rn}$, $T_{SIF4rs}$, $T_{SIF4LAI}$, and $T_{SIF4An}$).

| | WW Morning | | WL Morning | | WW Afternoon | | WL Afternoon | |
|---|---|---|---|---|---|---|---|---|
| Approach | $r^2$ | *RMSE* | $r^2$ | *RMSE* | $r^2$ | *RMSE* | $r^2$ | *RMSE* |
| $T_{PM}$ | 0.80 | 0.22 | 0.79 | 0.23 | 0.28 | 0.39 | 0.06 | 0.30 |
| $T_{BB}$ | 0.79 | 0.24 | 0.75 | 0.26 | 0.27 | 0.42 | 0.05 | 0.32 |
| $T_{SIF4T}$ | 0.31 | 0.21 | 0.32 | 0.29 | 0.22 | 0.38 | 0.48 | 0.35 |
| $T_{SIFRn}$ | 0.78 | 0.19 | 0.83 | 0.25 | 0.12 | 0.36 | 0.0001 | 0.32 |
| $T_{SIF4rs}$ | 0.90 | 0.21 | 0.74 | 0.25 | 0.48 | 0.36 | 0.19 | 0.29 |
| $T_{SIF4LAI}$ | 0.79 | 0.22 | 0.74 | 0.25 | 0.30 | 0.41 | 0.07 | 0.32 |
| $T_{SIF4An}$ | 0.76 | 0.22 | 0.77 | 0.24 | 0.24 | 0.40 | 0.04 | 0.30 |

evolving water limitation (i.e. an average T decrease of 3.5 %) related to a 60 % reduced volumetric soil moisture at the end of the experiment (cf. Damm et al., 2022). The observed sensitivity of RS informed standard T approaches for water limitation is in agreement with another study addressing T dynamics at coarser scale (Ahmed et al., 2021).

We evaluated the relative effect of SIF in T modeling and found closest agreement of the standard approaches with $T_{SIF4An}$, followed by $T_{SIF4LAI}$ and $T_{SIF4rs}$ (c.f. Fig. 7). This indicates the smallest effects of SIF on T estimates when replacing $A_n$, LAI and $r_s$ in the PM and BBL approaches. A possible explanation for this is the underlying approximation level, while in all three cases only the $r_s$ parameter of the PM modelling framework was modified and the specific value range during the experiment likely caused small importance in the PM and BBL equations. Likewise, replacing T with SIF resulted in largest relative differences compared to the standard T approaches, since SIF approximates in this case all, the energy, atmospheric and biological constraints on T.

The relative effect does not allow conclusions whether the use of SIF increased the accuracy of T estimates under water limited conditions or not. We therefore compared modelled T against a LST based reference T estimate. The best agreement with the LST based T estimates was observed for $T_{SIF4rs}$ (via smallest RMSE), $T_{SIF4An}$ (via highest $r^2$) and $T_{SIF4LAI}$ (via smaller RSME and higher $r^2$), while for these cases SIF was used to approximate stomatal conductance indirectly (i.e. via $A_n$ in BBL and LAI in PM) or directly (i.e. via $r_s$ in the PM model). This could indicate that $r_s$ is in fact an interesting entry point of SIF in T modelling. This general finding is in agreement with the studies by Shan et al. (2019, 2021), that also suggest connecting SIF with stomatal conductance. Nevertheless, our results do not allow ranking the best suited strategies to ingest SIF in T modelling.

Recent studies conclude on the importance of multi-sensor approaches to account for the individual underlying processes and plant adaptation mechanisms that act at different spatial and temporal scales when aiming to estimate T (e.g. Damm et al., 2018, 2022; Jonard et al., 2020). Results derived from our short-term experiment with subtle changes of soil water availability seem to confirm this finding: The approximation of individual parameters of the PM and BBL equations with SIF resulted in a higher agreement between SIF and LST based T estimates compared to the use of SIF as single proxy for T. This finding differs compared to recent studies that found an overall good performance for SIF as single proxy of T (Lu et al., 2018; Maes et al. 2020), indicating a scale dependency of SIF-T relationships via related spatial–temporal dynamics of T, SIF and underlying abiotic and biotic factors. In fact, we observed short-term changes in T in a structurally almost non-changing canopy, while existing studies investigated coarser temporal and spatial scales and covered larger gradients of T driving factors including canopy structure (Lu et al., 2018; Maes et al., 2020).

On a related note, it is important to make aware of the different temporal process lengths and underlying mechanisms determining dynamics in LAI and SIF. In fact, we only had a slight change of structural plant properties over the course of the experiment (small wilting effects, small increase of LAI in both canopy areas), while irradiance, thus SIF, varied more substantial. Since we pooled data that were observed under comparable conditions (i.e. morning and afternoon), we could avoid unrealistic sensitivities of SIF approximated LAI, thus $T_{SIF4LAI}$. We consider it important to harmonize length scales of parameters when they differ from SIF. Furthermore, considerations on the empirical relationship between SIF and T considering process lengths of approximated biotic and abiotic parameters is needed to elaborate on the best use of SIF and its representativeness for short- and long-term changes in plant water relations.

The comparison of all RS-based T estimates (i.e. standard approaches and SIF experiments) with independent $T_{SAP\text{-}flow}$ measurements indicates similar temporal dynamics and general T differences between the WW and WL treatment. However, we observe a 28 % overestimation of T for all RS approaches for both, the WW and WL areas, that hinders further conclusions on the most suited RS approach in relation to $T_{SAP\text{-}flow}$. Given the rather homogenous plants in the maize canopy, the small standard deviation of retrieved $T_{SAP\text{-}flow}$ (cf. Damm et al, 2022) and the fact that we used an established approach to measure $T_{SAP\text{-}flow}$, we consider the number of ten SAP gauges per treatment as sufficient and the accuracy of retrieved $T_{SAP\text{-}flow}$ as reliable. The 28 % offset is likely caused by the fundamental difference between RS and in situ approaches. The xylematic sap flow is measured at the stem base and includes both T and plant water storage. The latter process is neither considered in the PM equation nor measured with SIF because both focus on instantaneous data. Therefore, the contrasting mismatch becomes more evident during rapid T changes (Peressotti and Ham, 1996). Further, $T_{SAP\text{-}flow}$ in the morning is lower than T due to de-hydration, and higher compared to T in the evening due to re-hydration. T dynamics can be additionally driven by factors not impacting sap flow. Certainly, also local variability in plant density, LAI, and soil water retention curves could contribute to a dynamic in estimated $T_{SAP\text{-}flow}$ (Jara et al., 1998) that alters their representativeness for the entire canopy. Considering RS, the specific top-view perspective of RS representing the outer canopy area remains less sensitive for lower canopy layers (Damm et al., 2020). Therefore, RS-based T estimates will likely differ from established in situ T measurements (e.g. sap flow and eddy flux) in terms of value ranges and timing. Additional experimental and modelling research is needed to evaluate whether the observed 28 % bias is robust or changes across canopies and ecosystem types. Since we use SAP data only as independent context to interpret RS based T dynamics, observed bias does not affect the main outcome of our results, i.e. the observed RS based T dynamics and the assessment of relative and absolute effects of SIF in T modelling.

### 4.2. Reliability of this study

The reliability and representativeness of our findings depend on the input data and made assumptions. We used high resolution airborne data and applied established processing schemes for data product retrieval and, thus, could minimize related uncertainties (Hanuš et al., 2016; Rascher et al., 2015; Siegmann et al., 2019). Concerning the evaluation of absolute T accuracy, we used a RS-based LST proxy and in situ sap flow data. Previous studies showed that LST (downscaled and disaggregated) can be used for actual ET estimates (Bisquert et al., 2016; Jiang and Weng, 2017; Olivera-Guerra et al., 2017). Other studies have highlighted the feasibility, importance and positive impact of LST for ET modeling (Mahour et al., 2017; Sun et al., 2016). This indicates that derived relative differences between the LST based T estimates and the implemented standard and SIF-based experiments can be considered rather reliable, while statements on the absolute accuracy must be still interpreted with care. The additional evaluation of modelled T with independent sap flow-based measured T data provides complementary insight on relative and absolute accuracy. Fundamental differences between sap flow measurements and RS approaches, however, limit our ability to make statements on the absolute accuracy of evaluated T approaches.

In terms of our modeling setup, we used the established PM and BBL approaches for calculating standard T. Studies have shown that the PM equation was capable of considering the most crucial variables for T dynamics (e.g. Allen, 2005; Langensiepen et al., 2009), and the BBL equation is robust for modeling $g_s$, and related $r_s$ (Leuning, 1995). Despite the reliability of these modelling frameworks, some unavoidable limitations can compromise T estimates. A main problem lies, for example, in the practical necessity to use data with diverse spatial resolution and representativeness for model parameterization, e.g. non-spatial meteorological data vs spatially resolved data for structural variables. Nevertheless, our experimental results showed that T estimates with and without SIF provide plausible results under increasing water limitation, which is also evidenced by the comparison with independent sap flow-based T measurements.

We simplified the relationships between SIF and the different model parameters, i.e. the application of the unity-based normalization assumes linearity between SIF and individual parameters. However, SIF and $A_n$ were found to be hyperbolically related for large ranges of SIF and $A_n$ (i.e. Damm et al., 2015a; Gu et al., 2019; Liu et al., 2022). In fact, applying a non-linear saturating relationship between SIF and $A_n$ would result in a higher effect of SIF at low values and a lower effect of SIF at middle and higher values compared to the used linearity assumption. It must be noted that our experiment in the established maize canopy lasted only one week, with SIF values in the order of 1–2 mW $m^{-2}$ $nm^{-1}$ $sr^{-1}$ and we separatly pooled morning and afternoon data that were acquired under comparable light conditions. This means that value ranges for $A_n$, $R_n$, $r_s$ were relatively small so that the linearity assumption should be still reasonable. For LAI, we investigated data with a larger value range (i.e. 2–6 $m^2$ $m^{-2}$) but only small deviations of SIF-LAI relationships from linearity were reported in a recent modelling study (Damm et al., 2021). Considering more representative relationships would be ideal, but with the existing data it is impossible to derive them, and any assumptions would again introduce uncertainties. Further, since our results show expectedly a large dependence on the level of approximation (i.e. from replacing T by SIF or only individual model parameter) derived conclusions are not affected by the linearity assumption and stay robust.

### 4.3. Towards mechanistic SIF-based T assessments

Relationships between SIF and T greatly vary across vegetation types, climate and time due to individual sensitivities of both variables to underlying abiotic and biotic environmental factors (Maes et al., 2020). Several studies therefore suggest multi-data approaches to account for commonly applied assumptions in ET modeling and to consider the individual spatial and temporal dynamics of involved processes and used parameters (Damm et al., 2018; Jonard et al., 2020). In this context, the use of mechanistic soil–plant-atmosphere continuum (SPAC) models (e.g. García-Tejera et al., 2017; Tuzet et al., 2003) becomes interesting to possibly advance the use of SIF in T modelling. SPAC models offer the possibility to account for the limitation and distribution of soil water (García-Tejera et al., 2017) aside atmospheric and plant variables and processes, and allow moving towards more mechanistic descriptions of plant-water relations (Damm et al., 2018). SPAC like modelling concepts are already embedded in models like CLM5 (Bonan et al., 2014) to facilitate large scale approaches and enable consistent assessments of plant-water interactions across observational scales. Another important aspect concerning the refinement of modelling approaches is to account for different spatial dynamics of surface dryness (via stomatal conductance) and atmospheric dryness (via VPD and other micrometeorological variables) and to realistically represent them in models, particularly over complex structured landscapes with large contrasts of land cover. Also, the elastic behavior of plants including their transport capacity and ability to temporarily store water requires further attention.

We consider it important to include diverse in situ reference T measurements (e.g. EC flux measurements) in the experimental design of studies aiming to advance T modelling approaches. Observed and discussed differences between modelled RS and SAP-based T estimates suggest the need for additional refinements to better integrate and interlink both complementary and relevant approaches. In this context, additional developments of in situ T measurement strategies, (cf. Kool et al., 2014; Paul-Limoges et al., 2022; Paul-Limoges et al., 2020; Stoy et al., 2019), are needed to facilitate the exploitation, development and validation of mechanistic modelling approaches.

## 5. Conclusion

New functional vegetation information such as SIF complement existing observational approaches to assess dynamics of complex ecosystem processes (e.g. T) in response to evolving environmental stress like soil water limitation. We conclude that among the investigated approaches, linking SIF in various ways with the $r_s$ parameter of the PM-BBL modelling frameworks shows an interesting trade-off between a balanced effect on established T modelling and potential to increase the agreement between SIF based T estimates and T derived from established LST based approaches. We recommend further field and data experiments covering heterogeneous vegetation canopies and environmental stress types over longer time periods to assess sensitivity limits of SIF-based approaches for T modelling. Further advancement to mechanistically integrate SIF in models is important to fully exploit the potential of SIF and obtain additional insights for advancing T assessments at ecosystem scale. We observe a 28 % bias between RS and in situ based T estimates. We conclude on the importance to combine such independent observations of complex ecosystem gas exchange but also on the need for studies and methods to better integrate T estimates derived from such complementary approaches.

## Declaration of Competing Interest

The authors declare that they have no known competing financial interests or personal relationships that could have appeared to influence

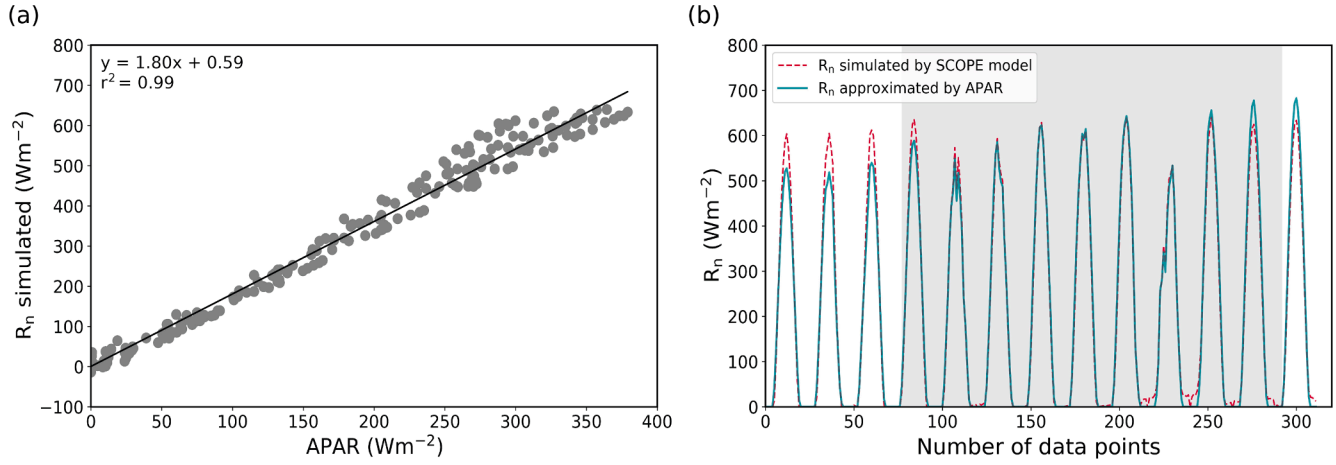


**Fig. A1.** Agreement between absorbed photosynthetic active radiation (APAR) and net radiation ($R_n$) simulated by the SCOPE model. SCOPE was parameterized with ERA-5 data (Muñoz-Sabater et al., 2021) and in situ measurements. (a) Scatterplot showing the agreement between APAR and $R_n$ before scaling. (b) The diurnal cycles of modeled $R_n$ and $R_n$ approximated by APAR at hourly time intervals. The shaded area indicates the measurement period from 16 to 24 June 2019.

**Table A1**
Temporal changes (mean ± standard deviation) of modeled transpiration (T) in $mmh^{-1}$ by two standard methods ($T_{PM}$, $T_{BB}$) and five sun-induced chlorophyll fluorescence (SIF)-based approaches ($T_{SIF4T}$, $T_{SIF4Rn}$, $T_{SIF4rs}$, $T_{SIF4LAI}$, & $T_{SIF4An}$) for the well-watered (WW) and the water-limited (WL) area. The six selected data equal the visualizations in Fig. 3.

| T [$mmhr^{-1}$] | | 16-06-2019 11:37 | 17-06-2019 11:33 | 18-06-2019 11:26 | 19-06-2019 10:34 | 23-06-2019 11:28 | 24-06-2019 11:17 |
|---|---|---|---|---|---|---|---|
| $T_{PM}$ | WW | 0.75 ± 0.04 | 0.83 ± 0.05 | 0.87 ± 0.04 | 0.77 ± 0.03 | 0.86 ± 0.02 | 0.89 ± 0.02 |
| | WL | 0.66 ± 0.05 | 0.74 ± 0.05 | 0.77 ± 0.05 | 0.71 ± 0.03 | 0.74 ± 0.04 | 0.76 ± 0.05 |
| $T_{BB}$ | WW | 0.79 ± 0.04 | 0.85 ± 0.04 | 0.89 ± 0.03 | 0.79 ± 0.02 | 0.88 ± 0.02 | 0.91 ± 0.02 |
| | WL | 0.71 ± 0.04 | 0.77 ± 0.05 | 0.81 ± 0.04 | 0.73 ± 0.03 | 0.77 ± 0.04 | 0.79 ± 0.05 |
| $T_{SIF4T}$ | WW | 0.78 ± 0.05 | 0.82 ± 0.04 | 0.80 ± 0.05 | 0.71 ± 0.04 | 0.89 ± 0.05 | 0.89 ± 0.04 |
| | WL | 0.77 ± 0.04 | 0.79 ± 0.04 | 0.79 ± 0.04 | 0.71 ± 0.03 | 0.87 ± 0.04 | 0.83 ± 0.04 |
| $T_{SIF4Rn}$ | WW | 0.71 ± 0.03 | 0.79 ± 0.03 | 0.81 ± 0.03 | 0.73 ± 0.03 | 0.82 ± 0.03 | 0.86 ± 0.03 |
| | WL | 0.68 ± 0.03 | 0.76 ± 0.02 | 0.78 ± 0.02 | 0.71 ± 0.02 | 0.77 ± 0.03 | 0.79 ± 0.03 |
| $T_{SIF4rs}$ | WW | 0.72 ± 0.02 | 0.79 ± 0.03 | 0.82 ± 0.02 | 0.74 ± 0.02 | 0.78 ± 0.01 | 0.81 ± 0.01 |
| | WL | 0.66 ± 0.03 | 0.73 ± 0.03 | 0.76 ± 0.03 | 0.71 ± 0.02 | 0.70 ± 0.03 | 0.73 ± 0.03 |
| $T_{SIF4LAI}$ | WW | 0.75 ± 0.04 | 0.83 ± 0.04 | 0.86 ± 0.03 | 0.75 ± 0.02 | 0.85 ± 0.02 | 0.88 ± 0.02 |
| | WL | 0.68 ± 0.04 | 0.76 ± 0.04 | 0.78 ± 0.04 | 0.70 ± 0.02 | 0.76 ± 0.03 | 0.77 ± 0.04 |
| $T_{SIF4An}$ | WW | 0.76 ± 0.04 | 0.83 ± 0.05 | 0.86 ± 0.04 | 0.77 ± 0.03 | 0.87 ± 0.02 | 0.89 ± 0.02 |
| | WL | 0.68 ± 0.04 | 0.75 ± 0.05 | 0.77 ± 0.04 | 0.71 ± 0.03 | 0.75 ± 0.04 | 0.76 ± 0.05 |

the work reported in this paper.

## Acknowledgment

We would like to thank the team and all the people involved in the FlexSense campaign 2019. We would like to thank the HyPlant team for operating and pre-processing the HyPlant data. We thank the team of JB-Hyperspectral for assistance in installing the FloX instrument. We would also like to acknowledge all the financing organizations for this research. Airborne acquisition and partly data pre-processing were financed by the European Space Agency (ESA) in the frame of the FLEXSense campaign (ESA Contract No. 4000125402/18/NL/NA), the Photoproxy campaign (ESA contract No. 4000125731/19/NL/LF), and the Surf-Sense campaign (ESA contract No. 4000125840/18/NL/LF). ERA-5 data was downloaded from the Copernicus Climate Change Service (C3S) Climate Data Store. A. Damm was supported by a grant of the Swiss National ScienceFoundation (SNSF, Fluo4Eco, contract no 197243). Lastly, we would like to thank anonymous reviewers for their important and constructive comments during the review process.

## Appendix A

Due to lack of relevant data to parameterize Eq. (2) and calculate net radiation ($R_n$), we followed a simpler approach making use of an empirically found and temporarily valid relationship between absorbed photosynthetic active radiation (APAR) and $R_n$. Since $R_n$ is determined by short-wave solar radiation (SW) represented by APAR and long-wave radiation (LW), $R_n$ estimates based on APAR typically underestimate $R_n$ and are prone to uncertainties since the LW dynamics are not considered. We established a sensitivity analysis to quantify the uncertainty related to our simplified APAR based $R_n$ estimate.

For the sensitivity analysis, we collected hourly ERA-5 data (Muñoz-Sabater et al., 2021) from the measurement period (13–25 June 2019), particularly, down-welling solar-radiation ($SW_{in}$), down-welling long-wave radiation ($LW_{in}$), wind speed, surface pressure, and air temperature.

These re-analyzed data together with in situ measured chlorophyll content, leaf area index (LAI), and canopy height were used to parameterize the SCOPE model, version 1.71 (van der Tol et al., 2009) to simulate APAR and $R_n$. The direct comparison with modelled $R_n$ reveals that an APAR based $R_n$ estimate underestimates by a factor of 1.8 (Fig. A.1). After applying the scaling factor, we observe a good agreement ($r^2$ of 0.98) and an overall root mean squared error (RMSE) of 24.09 $Wm^{-2}$, corresponding to an overall percentage error of 11.35% during the observational period (Fig. A.1).

## Appendix B

(Table A1)

## References

Ahmed, K.R., Paul-Limoges, E., Rascher, U., Damm, A., 2021. A first assessment of the 2018 European drought impact on ecosystem evapotranspiration. Remote Sens. 13, 1–17. https://doi.org/10.3390/rs13010016.

Allen, R., 2005. Penman – Monteith Equation. Encycl. Soils Environ. 180–188.

Allen, R.G., Pereira, L.S., Raes, D., Smith, M., Ab, W., 1998. Crop evapotranspiration - Guidelines for computing crop water requirements. FAO Irrig. Drain. Pap. 56, 300. https://doi.org/10.1016/j.eja.2010.12.001.

Anderegg, W.R.L., Berry, J.A., Smith, D.D., Sperry, J.S., Anderegg, L.D.L., Field, C.B., 2012. The roles of hydraulic and carbon stress in a widespread climate-induced forest die-off. Proc. Natl. Acad. Sci. U. S. A. 109, 233–237. https://doi.org/10.1073/pnas.1107891109.

Ball, J.T., Woodrow, I.E., Berry, J.A., 1987. A Model Predicting Stomatal Conductance and Its Contribution to the Control of Photosynthesis Under Different Environmental Conditions. Prog. Photosynth. Res. https://doi.org/10.1007/978-94-017-0519-6_48.

Bisquert, M., Sánchez, J.M., López-Urrea, R., Caselles, V., 2016. Estimating high resolution evapotranspiration from disaggregated thermal images. Remote Sens. Environ. 187, 423–433. https://doi.org/10.1016/j.rse.2016.10.049.

Bonan, G.B., 2008. Forests and climate change: Forcings, feedbacks, and the climate benefits of forests. Science 80-.). 320, 1444–1449. https://doi.org/10.1126/science.1155121.

Bonan, G.B., Williams, M., Fisher, R.A., Oleson, K.W., 2014. Modeling stomatal conductance in the earth system: Linking leaf water-use efficiency and water transport along the soil-plant-atmosphere continuum. Geosci. Model Dev. 7, 2193–2222. https://doi.org/10.5194/gmd-7-2193-2014.

Campbell, G.S., Norman, J.M., 1998. An Introduction to Environmental Biophysics, Second. ed. Springer Science+Business Media New York. https://doi.org/10.1007/978-1-4612-1626-1.

Cogliati, S., Verhoef, W., Kraft, S., Sabater, N., Alonso, L., Vicent, J., Moreno, J., Drusch, M., Colombo, R., 2015. Retrieval of sun-induced fluorescence using advanced spectral fitting methods. Remote Sens. Environ. 169, 344–357. https://doi.org/10.1016/j.rse.2015.08.022.

Damm, A., Guanter, L., Paul-Limoges, E., van der Tol, C., Hueni, A., Buchmann, N., Eugster, W., Ammann, C., Schaepman, M.E., 2015a. Far-red sun-induced chlorophyll fluorescence shows ecosystem-specific relationships to gross primary production: An assessment based on observational and modeling approaches. Remote Sens. Environ. 166, 91–105. https://doi.org/10.1016/j.rse.2015.06.004.

Damm, A., Guanter, L., Verhoef, W., Schläpfer, D., Garbari, S., Schaepman, M.E., 2015b. Impact of varying irradiance on vegetation indices and chlorophyll fluorescence derived from spectroscopy data. Remote Sens. Environ. 156, 202–215. https://doi.org/10.1016/j.rse.2014.09.031.

Damm, A., Paul-Limoges, E., Haghighi, E., Simmer, C., Morsdorf, F., Schneider, F.D., van der Tol, C., Migliavacca, M., Rascher, U., 2018. Remote sensing of plant-water relations: An overview and future perspectives. J. Plant Physiol. 227, 3–19. https://doi.org/10.1016/j.jplph.2018.04.012.

Damm, A., Paul-Limoges, E., Kükenbrink, D., Bachofen, C., Morsdorf, F., 2020. Remote sensing of forest gas exchange: Considerations derived from a tomographic perspective. Glob. Chang. Biol. 26, 2717–2727. https://doi.org/10.1111/gcb.15007.

Damm, A., Cogliati, S., Colombo, R., Fritsche, L., Genangeli, A., Genesio, L., Hanus, J., Peressotti, A., Rademske, P., Rascher, U., Schuettemeyer, D., Siegmann, B., Sturm, J., Miglietta, F., 2022. Response times of remote sensing measured sun-induced chlorophyll fluorescence, surface temperature and vegetation indices to evolving soil water limitation in a crop canopy. Remote Sens. Environ. 273, 112957 https://doi.org/10.1016/j.rse.2022.112957.

Damm A., Haghighi E., Paul-Limoges E., Tol, C. van der, 2021. On the seasonal relation of sun-induced chlorophyll fluorescence and transpiration in a temperate mixed forest. Agric. For. Meteorol. 304–305, 108386. https://doi.org/10.1016/j.agrformet.2021.108386.

Dechant, B., Ryu, Y., Badgley, G., Zeng, Y., Berry, J.A., Zhang, Y., Goulas, Y., Li, Z., Zhang, Q., Kang, M., Li, J., Moya, I., 2020. Canopy structure explains the

relationship between photosynthesis and sun-induced chlorophyll fluorescence in crops. Remote Sens. Environ. 241 https://doi.org/10.1016/j.rse.2020.111733.
Frank, D., Reichstein, M., Bahn, M., Thonicke, K., Frank, D., Mahecha, M.D., Smith, P., van der Velde, M., Vicca, S., Babst, F., Beer, C., Buchmann, N., Canadell, J.G., Ciais, P., Cramer, W., Ibrom, A., Miglietta, F., Poulter, B., Rammig, A., Seneviratne, S.I., Walz, A., Wattenbach, M., Zavala, M.A., Zscheischler, J., 2015. Effects of climate extremes on the terrestrial carbon cycle: Concepts, processes and potential future impacts. Glob. Chang. Biol. 21, 2861–2880. https://doi.org/10.1111/gcb.12916.
García-Tejera, O., López-Bernal, Á., Testi, L., Villalobos, F.J., 2017. A soil-plant-atmosphere continuum (SPAC) model for simulating tree transpiration with a soil multi-compartment solution. Plant Soil 412, 215–233. https://doi.org/10.1007/s11104-016-3049-0.
Gentine, P., Green, J.K., Guérin, M., Humphrey, V., Seneviratne, S.I., Zhang, Y., Zhou, S., 2019. Coupling between the terrestrial carbon and water cycles - A review. Environ. Res. Lett. 14 https://doi.org/10.1088/1748-9326/ab22d6.
Gharun, M., Hörtnagl, L., Paul-Limoges, E., Ghiasi, S., Feigenwinter, I., Burri, S., Marquardt, K., Etzold, S., Zweifel, R., Eugster, W., Buchmann, N., 2020. Physiological response of Swiss ecosystems to 2018 drought across plant types and elevation: Summer 2018 drought in Switzerland. Philos. Trans. R. Soc. B Biol. Sci. 375 https://doi.org/10.1098/rstb.2019.0521.
Gong, X., Liu, H., Sun, J., Gao, Y., Zhang, X., Jha, S.K., Zhang, H., Ma, X., Wang, W., 2017. A proposed surface resistance model for the Penman-Monteith formula to estimate evapotranspiration in a solar greenhouse. J. Arid Land 9, 530–546. https://doi.org/10.1007/s40333-017-0020-8.
Green, S.R., McNaughton, K.G., Greer, D.H., McLeod, D.J., 1995. Measurement of the increased PAR and net all-wave radiation absorption by an apple tree caused by applying a reflective ground covering. Agric. For. Meteorol. 76, 163–183. https://doi.org/10.1016/0168-1923(95)02228-P.
Gu, L., Han, J., Wood, J.D., Chang, C.Y.Y., Sun, Y., 2019. Sun-induced Chl fluorescence and its importance for biophysical modeling of photosynthesis based on light reactions. New Phytol. 223, 1179–1191. https://doi.org/10.1111/nph.15796.
Guanter, L., Zhang, Y., Jung, M., Joiner, J., Voigt, M., Berry, J.A., Frankenberg, C., Huete, A.R., Zarco-Tejada, P., Lee, J.E., Moran, M.S., Ponce-Campos, G., Beer, C., Camps-Valls, G., Buchmann, N., Gianelle, D., Klumpp, K., Cescatti, A., Baker, J.M., Griffis, T.J., 2014. Global and time-resolved monitoring of crop photosynthesis with chlorophyll fluorescence. Proc. Natl. Acad. Sci. U. S. A. 111 https://doi.org/10.1073/pnas.1320008111.
Hanuš, J., Fabiánek, T., Fajmon, L., 2016. Potential of airborne imaging spectroscopy at CzechGlobe. Int. Arch. Photogramm. Remote Sens. Spat. Inf. Sci. - ISPRS Arch. 2016-Janua, 15–17. https://doi.org/10.5194/isprsarchives-XLI-B1-15-2016.
He, Q.L., Xiao, J.L., Shi, W.Y., 2022. Responses of Terrestrial Evapotranspiration to Extreme Drought: A Review. Water (Switzerland) 14. https://doi.org/10.3390/w14233847.
Hilker, T., Hall, F.G., Coops, N.C., Collatz, J.G., Black, T.A., Tucker, C.J., Sellers, P.J., Grant, N., 2013. Remote sensing of transpiration and heat fluxes using multi-angle observations. Remote Sens. Environ. 137, 31–42. https://doi.org/10.1016/j.rse.2013.05.023.
Jara, J., Stockle, C.O., Kjelgaard, J., 1998. Measurement of evapotranspiration and its components in a corn (Zea Mays L.) field. Agric. For. Meteorol. 92, 131–145. https://doi.org/10.1016/S0168-1923(98)00083-5.
Jiang, Y., Weng, Q., 2017. Estimation of hourly and daily evapotranspiration and soil moisture using downscaled LST over various urban surfaces. GIScience Remote Sens. 54, 95–117. https://doi.org/10.1080/15481603.2016.1258971.
Jonard, F., De Cannière, S., Brüggemann, N., Gentine, P., Short Gianotti, D.J., Lobet, G., Miralles, D.G., Montzka, C., Pagán, B.R., Rascher, U., Vereecken, H., 2020. Value of sun-induced chlorophyll fluorescence for quantifying hydrological states and fluxes: Current status and challenges. Agric. For. Meteorol. 291, 108088 https://doi.org/10.1016/j.agrformet.2020.108088.
Kool, D., Agam, N., Lazarovitch, N., Heitman, J.L., Sauer, T.J., Ben-Gal, A., 2014. A review of approaches for evapotranspiration partitioning. Agric. For. Meteorol. 184, 56–70. https://doi.org/10.1016/j.agrformet.2013.09.003.
Langensiepen, M., Fuchs, M., Bergamaschi, H., Moreshet, S., Cohen, Y., Wolff, P., Jutzi, S. C., Cohen, S., Rosa, L.M.G., Li, Y., Fricke, T., 2009. Quantifying the uncertainties of transpiration calculations with the Penman-Monteith equation under different climate and optimum water supply conditions. Agric. For. Meteorol. 149, 1063–1072. https://doi.org/10.1016/j.agrformet.2009.01.001.
Leuning, R., 1995. A critical appraisal of a combined stomatal-photosynthesis model for C3 plants. Plant. Cell Environ. 18, 339–355. https://doi.org/10.1111/j.1365-3040.1995.tb00370.x.
Liang, S., 2004. Quantitative Remote Sensing of Land Surfaces. First Edit. ed. John Wilcy & Sons. https://doi.org/10.1002/047172372X.
Liu, Z., Zhao, F., Liu, X., Yu, Q., Wang, Y., Peng, X., Cai, H., Lu, X., 2022. Direct estimation of photosynthetic CO2 assimilation from solar-induced chlorophyll fluorescence (SIF). Remote Sens. Environ. 271, 112893 https://doi.org/10.1016/j.rse.2022.112893.
Lu, X., Liu, Z., An, S., Miralles, D.G., Maes, W., Liu, Y., Tang, J., 2018. Potential of solar-induced chlorophyll fluorescence to estimate transpiration in a temperate forest. Agric. For. Meteorol. 252, 75–87. https://doi.org/10.1016/j.agrformet.2018.01.017.
Maes, W.H., Pagán, B.R., Martens, B., Gentine, P., Guanter, L., Steppe, K., Verhoest, N.E. C., Dorigo, W., Li, X., Xiao, J., Miralles, D.G., 2020. Sun-induced fl uorescence closely linked to ecosystem transpiration as evidenced by satellite data and radiative transfer models. Remote Sens. Environ. 249, 112030 https://doi.org/10.1016/j.rse.2020.112030.
Mahour, M., Tolpekin, V., Stein, A., Sharifi, A., 2017. A comparison of two downscaling procedures to increase the spatial resolution of mapping actual evapotranspiration. ISPRS J. Photogramm. Remote Sens. 126, 56–67. https://doi.org/10.1016/j.isprsjprs.2017.02.004.
Meroni, M., Busetto, L., Colombo, R., Guanter, L., Moreno, J., Verhoef, W., 2010. Performance of Spectral Fitting Methods for vegetation fluorescence quantification. Remote Sens. Environ. 114, 363–374. https://doi.org/10.1016/j.rse.2009.09.010.
Mohammed, G.H., Colombo, R., Middleton, E.M., Rascher, U., van der Tol, C., Nedbal, L., Goulas, Y., Pérez-Priego, O., Damm, A., Meroni, M., Joiner, J., Cogliati, S., Verhoef, W., Malenovský, Z., Gastellu-Etchegorry, J.P., Miller, J.R., Guanter, L., Moreno, J., Moya, I., Berry, J.A., Frankenberg, C., Zarco-Tejada, P.J., 2019. Remote sensing of solar-induced chlorophyll fluorescence (SIF) in vegetation: 50 years of progress. Remote Sens. Environ. 231, 111177 https://doi.org/10.1016/j.rse.2019.04.030.
Monteith, J.L., 1965. Evaporation and environment. Symp. Soc. Exp, Biol.
Muñoz-Sabater, J., Dutra, E., Agustí-Panareda, A., Albergel, C., Arduini, G., Balsamo, G., Boussetta, S., Choulga, M., Harrigan, S., Hersbach, H., Martens, B., Miralles, D.G., Piles, M., Rodríguez-Fernández, N.J., Zsoter, E., Buontempo, C., Thépaut, J.N., 2021. ERA5-Land: A state-of-the-art global reanalysis dataset for land applications. Earth Syst. Sci. Data 13, 4349–4383. https://doi.org/10.5194/essd-13-4349-2021.
Oliphant, A., Susan, C., Grimmond, B., Schmid, H.P., Wayson, C.A., 2006. Local-scale heterogeneity of photosynthetically active radiation (PAR), absorbed PAR and net radiation as a function of topography, sky conditions and leaf area index. Remote Sens. Environ. 103, 324–337. https://doi.org/10.1016/j.rse.2005.09.021.
Olivera-Guerra, L., Mattar, C., Merlin, O., Durán-Alarcón, C., Santamaría-Artigas, A., Fuster, R., 2017. An operational method for the disaggregation of land surface temperature to estimate actual evapotranspiration in the arid region of Chile. ISPRS J. Photogramm. Remote Sens. 128, 170–181. https://doi.org/10.1016/j.isprsjprs.2017.03.014.
Paul-Limoges, E., Revill, A., Maier, R., Buchmann, N., Damm, A., 2022. Insights for the Partitioning of Ecosystem Evaporation and Transpiration in Short-Statured Croplands. J. Geophys. Res. Biogeosciences 127. https://doi.org/https://doi. org/10.1029/2021JG006760.
Pagán, B.R., Maes, W.H., Gentine, P., Martes, B., Miralles, D.G., 2019. Exploring the Potential of Satellite Solar-Induced Fluorescence to Constrain Global Transpiration Estimates. Remote Sensing 11, 413. https://doi.org/10.3390/rs11040413.
Paul-Limoges, E., Wolf, S., Schneider, F.D., Longo, M., Moorcroft, P., Gharun, M., Damm, A., 2020. Partitioning evapotranspiration with concurrent eddy covariance measurements in a mixed forest. Agric. For. Meteorol. 280, 107786 https://doi.org/10.1016/j.agrformet.2019.107786.
Peng, Y., Gitelson, A.A., 2011. Application of chlorophyll-related vegetation indices for remote estimation of maize productivity. Agric. For. Meteorol. 151, 1267–1276. https://doi.org/10.1016/j.agrformet.2011.05.005.
Peng, Y., Gitelson, A.A., Keydan, G., Rundquist, D.C., Moses, W., 2011. Remote estimation of gross primary production in maize and support for a new paradigm based on total crop chlorophyll content. Remote Sens. Environ. 115, 978–989. https://doi.org/10.1016/j.rse.2010.12.001.
Penman, H.L., 1948. Natural evaporation from open water, hare soil and grass. Proc. R. Soc. Lond. A. Math. Phys. Sci. 193, 120–145. https://doi.org/10.1098/rspa.1948.0037.
Peressotti, A., Ham, J.M., 1996. A dual-heater gauge for measuring sap flow with an improved heat- balance method. Agron. J. 88, 149–155. https://doi.org/10.2134/agronj1996.00021962008800020006x.
Porcar-Castell, A., Malenovský, Z., Magney, T., Van Wittenberghe, S., Fernández-Marín, B., Maignan, F., Zhang, Y., Maseyk, K., Atherton, J., Albert, L.P., Robson, T. M., Zhao, F., Garcia-Plazaola, J.-I., Ensminger, I., Rajewicz, P.A., Grebe, S., Tikkanen, M., Kellner, J.R., Ihalainen, J.A., Rascher, U., Logan, B., 2021. Chlorophyll a fluorescence illuminates a path connecting plant molecular biology to Earth-system science. Nat. Plants 7, 998–1009. https://doi.org/10.1038/s41477-021-00980-4.
Ramonet, M., Ciais, P., Apadula, F., Bartyzel, J., Bastos, A., Bergamaschi, P., Blanc, P.E., Brunner, D., Caracciolo Di Torchiarolo, L., Calzolari, F., Chen, H., Chmura, L., Colomb, A., Conil, S., Cristofanelli, P., Cuevas, E., Curcoll, R., Delmotte, M., Di Sarra, A., Emmenegger, L., Forster, G., Frumau, A., Gerbig, C., Gheusi, F., Hammer, S., Haszpra, L., Hatakka, J., Hazan, L., Heliasz, M., Henne, S., Hensen, A., Hermansen, O., Keronen, P., Kivi, R., Komínková, K., Kubistin, D., Laurent, O., Laurila, T., Lavric, J. V., Lehner, I., Lehtinen, K.E.J., Leskinen, A., Leuenberger, M., Levin, I., Lindauer, M., Lopez, M., Myhre, C.L., Mammarella, I., Manca, G., Manning, A., Marek, M. V., Marklund, P., Martin, D., Meinhardt, F., Mihalopoulos, N., Mölder, M., Morgui, J.A., Necki, J., O'Doherty, S., O'Dowd, C., Ottosson, M., Philippon, C., Piacentino, S., Pichon, J.M., Plass-Duelmer, C., Resovsky, A., Rivier, L., Rodó, X., Sha, M.K., Scheeren, H.A., Sferlazzo, D., Spain, T.G., Stanley, K.M., Steinbacher, M., Trisolino, P., Vermeulen, A., Vítková, G., Weyrauch, D., Xueref-Remy, I., Yala, K., Yver Kwok, C., 2020. The fingerprint of the summer 2018 drought in Europe on ground-based atmospheric CO 2 measurements: Atmospheric CO 2 anomaly. Philos. Trans. R. Soc. B Biol. Sci. 375. https://doi.org/10.1098/rstb.2019.0513.
Rascher, U., Alonso, L., Burkart, A., Cilia, C., Cogliati, S., Colombo, R., Damm, A., Drusch, M., Guanter, L., Hanus, J., Hyvärinen, T., Julitta, T., Jussila, J., Kataja, K., Kokkalis, P., Kraft, S., Kraska, T., Matveeva, M., Moreno, J., Muller, O., Panigada, C., Pikl, M., Pinto, F., Prey, L., Pude, R., Rossini, M., Schickling, A., Schurr, U., Schüttemeyer, D., Verrelst, J., Zemek, F., 2015. Sun-induced fluorescence - a new probe of photosynthesis: First maps from the imaging spectrometer HyPlant. Glob. Chang. Biol. 21, 4673–4684. https://doi.org/10.1111/gcb.13017.
Reichstein, M., Bahn, M., Ciais, P., Frank, D., Mahecha, M.D., Seneviratne, S.I., Zscheischler, J., Beer, C., Buchmann, N., Frank, D.C., Papale, D., Rammig, A., Smith, P., Thonicke, K., Van Der Velde, M., Vicca, S., Walz, A., Wattenbach, M.,

2013. Climate extremes and the carbon cycle. Nature 500 (7462), 287–295. https://doi.org/10.1038/nature12350.

Reichstein, M., Tenhunen, J.D., Roupsard, O., Ourcival, J.M., Rambal, S., Miglietta, F., Peressotti, A., Pecchiari, M., Tirone, G., Valentini, R., 2002. Severe drought effects on ecosystem CO2 and H2O fluxes at three Mediterranean evergreen sites: Revision of current hypotheses? Glob. Chang. Biol. 8, 999–1017. https://doi.org/10.1046/j.1365-2486.2002.00530.x.

Ryu, Y., Berry, J.A., Baldocchi, D.D., 2019. What is global photosynthesis? History, uncertainties and opportunities. Remote Sens. Environ. 223, 95–114. https://doi.org/10.1016/j.rse.2019.01.016.

Sakuratani, T., 1981. A Heat Balance Method for Measuring Water Flux in the Stem of Intact Plants. J. Agric. Meteorol. 37, 9–17. https://doi.org/10.2480/agrmet.37.9.

Schimel, D., Schneider, F.D., Carbon, JPL, Ecosystem Participants, 2019. Flux towers in the sky: global ecology from space. New Phytologist 224 (2), 570–584. https://doi.org/10.1111/nph.15934.

Shan, N., Ju, W., Migliavacca, M., Martini, D., Guanter, L., Chen, J., Goulas, Y., Zhang, Y., 2019. Modeling canopy conductance and transpiration from solar-induced chlorophyll fluorescence. Agric. For. Meteorol. 268, 189–201. https://doi.org/10.1016/j.agrformet.2019.01.031.

Shan, N., Zhang, Y., Chen, J.M., Ju, W., Migliavacca, M., Peñuelas, J., Yang, X., Zhang, Z., Nelson, J.A., Goulas, Y., 2021. A model for estimating transpiration from remotely sensed solar-induced chlorophyll fluorescence. Remote Sens. Environ. 252 https://doi.org/10.1016/j.rse.2020.112134.

Siegmann, B., Alonso, L., Celesti, M., Cogliati, S., Colombo, R., Damm, A., Douglas, S., Guanter, L., Hanuš, J., Kataja, K., Kraska, T., Matveeva, M., Moreno, J., Muller, O., Pikl, M., Pinto, F., Vargas, J.Q., Rademske, P., Rodriguez-Morene, F., Sabater, N., Schickling, A., Schüttemeyer, D., Zemek, F., Rascher, U., 2019. The high-performance airborne imaging spectrometer HyPlant-from raw images to top-of-canopy reflectance and fluorescence products: Introduction of an automatized processing chain. Remote Sens. 11 https://doi.org/10.3390/rs11232760.

Sippel, S., Reichstein, M., Ma, X.L., Mahecha, M.D., Lange, H., Flach, M., Frank, D., 2018. Drought, Heat, and the Carbon Cycle. Current Climate Change Reports 4 (3), 266–286. https://doi.org/10.1007/s40641-018-0103-4.

Stoy, P.C., El-Madany, T.S., Fisher, J.B., Gentine, P., Gerken, T., Good, S.P., Klosterhalfen, A., Liu, S., Miralles, D.G., Perez-Priego, O., Rigden, A.J., Skaggs, T.H., Wohlfahrt, G., Anderson, R.G., Coenders-Gerrits, A.M.J., Jung, M., Maes, W.H., Mammarella, I., Mauder, M., Migliavacca, M., Nelson, J.A., Poyatos, R., Reichstein, M., Scott, R.L., Wolf, S., 2019. Reviews and syntheses: Turning the challenges of partitioning ecosystem evaporation and transpiration into opportunities. Biogeosciences 16, 3747–3775. https://doi.org/10.5194/bg-16-3747-2019.

Sun, Z., Wang, Q., Batkhishig, O., Ouyang, Z., 2016. Relationship between Evapotranspiration and land surface temperature under energy- and water-limited conditions in dry and cold climates. Adv. Meteorol. 2016 https://doi.org/10.1155/2016/1835487.

Toll, D.L., Shirey, D.A., Kimes, D.S., 1994. Using remotely sensed data to estimate surface albedo and absorbed photosynthetic active radiation. Int. Geosci. Remote Sens. Symp. 3, 1461–1463. https://doi.org/10.1109/igarss.1994.399469.

Tuzet, A., Perrier, A., Leuning, R., 2003. A coupled model of stomatal conductance, photosynthesis and transpiration. Plant, Cell Environ. 26, 1097–1116. https://doi.org/10.1046/j.1365-3040.2003.01035.x.

Van Der Tol, C., Verhoef, W., Timmermans, J., Verhoef, A., Su, Z., 2009. An integrated model of soil-canopy spectral radiances, photosynthesis, fluorescence, temperature and energy balance. Biogeosciences 6, 3109–3129. https://doi.org/10.5194/bg-6-3109-2009.

Wang, K., Liang, S., 2009. Estimation of daytime net radiation from shortwave radiation measurements and meteorological observations. J. Appl. Meteorol. Climatol. 48, 634–643. https://doi.org/10.1175/2008JAMC1959.1.

Wang, S., Zhang, Y., Ju, W., Wu, M., Liu, L., He, W., Peñuelas, J., 2022. Temporally corrected long-term satellite solar-induced fluorescence leads to improved estimation of global trends in vegetation photosynthesis during 1995–2018. ISPRS J. Photogramm. Remote Sens. 194, 222–234. https://doi.org/10.1016/j.isprsjprs.2022.10.018.

Wieneke, S., Ahrends, H., Damm, A., Pinto, F., Stadler, A., Rossini, M., Rascher, U., 2016. Airborne based spectroscopy of red and far-red sun-induced chlorophyll fluorescence: Implications for improved estimates of gross primary productivity. Remote Sens. Environ. 184, 654–667. https://doi.org/10.1016/j.rse.2016.07.025.

Xiao, J., Fisher, J.B., Hashimoto, H., Ichii, K., Parazoo, N.C., 2021. Emerging satellite observations for diurnal cycling of ecosystem processes. Nat. Plants 7, 877–887. https://doi.org/10.1038/s41477-021-00952-8.

Yebra, M., Van Dijk, A., Leuning, R., Huete, A., Guerschman, J.P., 2013. Evaluation of optical remote sensing to estimate actual evapotranspiration and canopy conductance. Remote Sens. Environ. 129, 250–261. https://doi.org/10.1016/j.rse.2012.11.004.

Zhang, F., Zhou, G., Nilsson, C., 2015. Remote estimation of the fraction of absorbed photosynthetically active radiation for a maize canopy in Northeast China. J. Plant Ecol. 8, 429–435. https://doi.org/10.1093/jpe/rtu027.